Cell Reports

Article

Topoisomerase 1-dependent R-loop deficiency drives accelerated replication and genomic instability

Graphical abstract

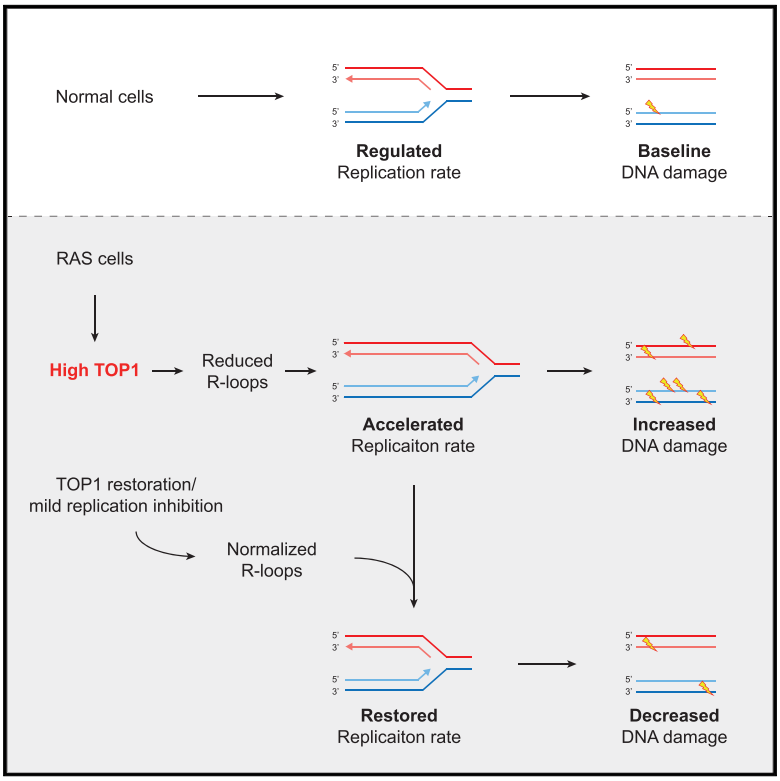

Highlights

- Increased TOP1 expression by mutated RAS reduces R loops
- Low R-loop levels promote accelerated replication and DNA damage
- TOP1 restoration or mild replication inhibition rescue DNA acceleration and damage
- High TOP1 expression is associated with replication mutagenesis in cancer

Authors

Dan Sarni, Sonia Barroso, Alon Shtrikman, Michal Irony-Tur Sinai, Yifat S. Oren, Andrés Aguilera, Batsheva Kerem

Correspondence

batshevak@savion.huji.ac.il

In brief

TOP1 deficiency increases R loops driving replication stress characterized by slow replication and DNA damage. Sarni et al. reveal that HRAS increases TOP1 and reduces R loops, causing accelerated replication and DNA damage, highlighting the importance of TOP1 equilibrium in regulating R-loop homeostasis to ensure faithful replication and genome integrity.

Sarni et al., 2022, Cell Reports *40*, 111397
September 27, 2022 © 2022 The Author(s).
https://doi.org/10.1016/j.celrep.2022.111397

CellPress

Cell Reports

CellPress
OPEN ACCESS

Article

Topoisomerase 1-dependent R-loop deficiency drives accelerated replication and genomic instability

Dan Sarni,[1] Sonia Barroso,[2] Alon Shtrikman,[1] Michal Irony-Tur Sinai,[1] Yifat S. Oren,[1] Andrés Aguilera,[2] and Batsheva Kerem[1,3,*]

[1]Department of Genetics, The Life Sciences Institute, The Hebrew University, Jerusalem 91904, Israel
[2]Department of Genome Biology, Andalusian Center of Molecular Biology and Regenerative Medicine CABIMER, Seville Universidad de Sevilla-CSIC-Universidad Pablo de Olavide, Seville, Spain
[3]Lead contact
*Correspondence: batshevak@savion.huji.ac.il
https://doi.org/10.1016/j.celrep.2022.111397

SUMMARY

DNA replication is a complex process tightly regulated to ensure faithful genome duplication, and its perturbation leads to DNA damage and genomic instability. Replication stress is commonly associated with slow and stalled replication forks. Recently, accelerated replication has emerged as a non-canonical form of replication stress. However, the molecular basis underlying fork acceleration is largely unknown. Here, we show that mutated HRAS activation leads to increased topoisomerase 1 (TOP1) expression, causing aberrant replication fork acceleration and DNA damage by decreasing RNA-DNA hybrids or R-loops. In these cells, restoration of TOP1 expression or mild replication inhibition rescues the perturbed replication and reduces DNA damage. Furthermore, TOP1 or RNaseH1 overexpression induces accelerated replication and DNA damage, highlighting the importance of TOP1 equilibrium in regulating R-loop homeostasis to ensure faithful DNA replication and genome integrity. Altogether, our results dissect a mechanism of oncogene-induced DNA damage by aberrant replication fork acceleration.

INTRODUCTION

DNA replication is a complex process that is tightly regulated to ensure faithful duplication of the genome. Various factors are involved in regulating replication, including origin licensing and firing, replication elongation rate, and termination (Conti et al., 2007; Fragkos et al., 2015). Under conditions that slow or stall replication fork progression (defined as replication stress), dormant origins are activated to allow completion of DNA synthesis to maintain genome integrity (Courbet et al., 2008; Ge et al., 2007). However, insufficient compensation of the perturbed DNA replication may lead to genome instability (Gaillard et al., 2015; Zeman and Cimprich, 2014). Several factors lead to replication stress, among them nucleotide deficiency, accumulation of RNA-DNA hybrids and DNA lesions (Gaillard et al., 2015; Zeman and Cimprich, 2014), all of which result in perturbed replication dynamics and increased genomic instability.

Genomic instability is a hallmark of cancer and a driver of tumorigenesis (Hanahan and Weinberg, 2011; Negrini et al., 2010). Aberrant activation of oncogenes and tumor suppressor genes induces replication stress, leading to accumulation of DNA damage and an increased tumorigenicity potential (Bartkova et al., 2006; Bester et al., 2011; Dominguez-Sola et al., 2007; Galanos et al., 2016; Di Micco et al., 2006). This stress is characterized by slow replication rate, fork stalling, activation of dormant origins, and even re-replication. However, several studies have found accelerated replication rates following alterations in expression of various genes including overexpression (OE) of the oncogene Spi-1 (Rimmele et al., 2010) and the cancer-associated gene ISG15 (Raso et al., 2020), downregulation of mRNA biogenesis genes involved in mRNA processing and export (Bhatia et al., 2014; Domínguez-Sánchez et al., 2011; Salas-Armenteros et al., 2017), depletion of origin-firing factors (Sedlackova et al., 2020; Zhong et al., 2013), and inhibition of poly(ADP-ribose) polymerase (PARP) (Maya-Mendoza et al., 2018; Sugimura et al., 2008). In most of these studies, accelerated replication was accompanied by DNA damage. However, whether the accelerated replication rate induces DNA damage, per se, and the molecular mechanism(s) underlying fork acceleration are largely unknown.

Here, we show that activation of the mutated HRAS (RAS) oncogene in pre-senescent cells increases topoisomerase 1 (TOP1) levels, leading to replication fork acceleration and DNA damage by decreasing R-loop levels. Restoration of TOP1 expression or mild replication inhibition in RAS-expressing cells restores normal R-loop levels, rescues the perturbed replication, and reduces DNA damage. We further show that OE of TOP1 causes aberrant replication fork acceleration and DNA damage, similar to the effect of TOP1 increase by RAS. Degradation of R-loops by OE of RNaseH1, independent of TOP1 OE, also

This is an open access article under the CC BY-NC-ND license (http://creativecommons.org/licenses/by-nc-nd/4.0/).

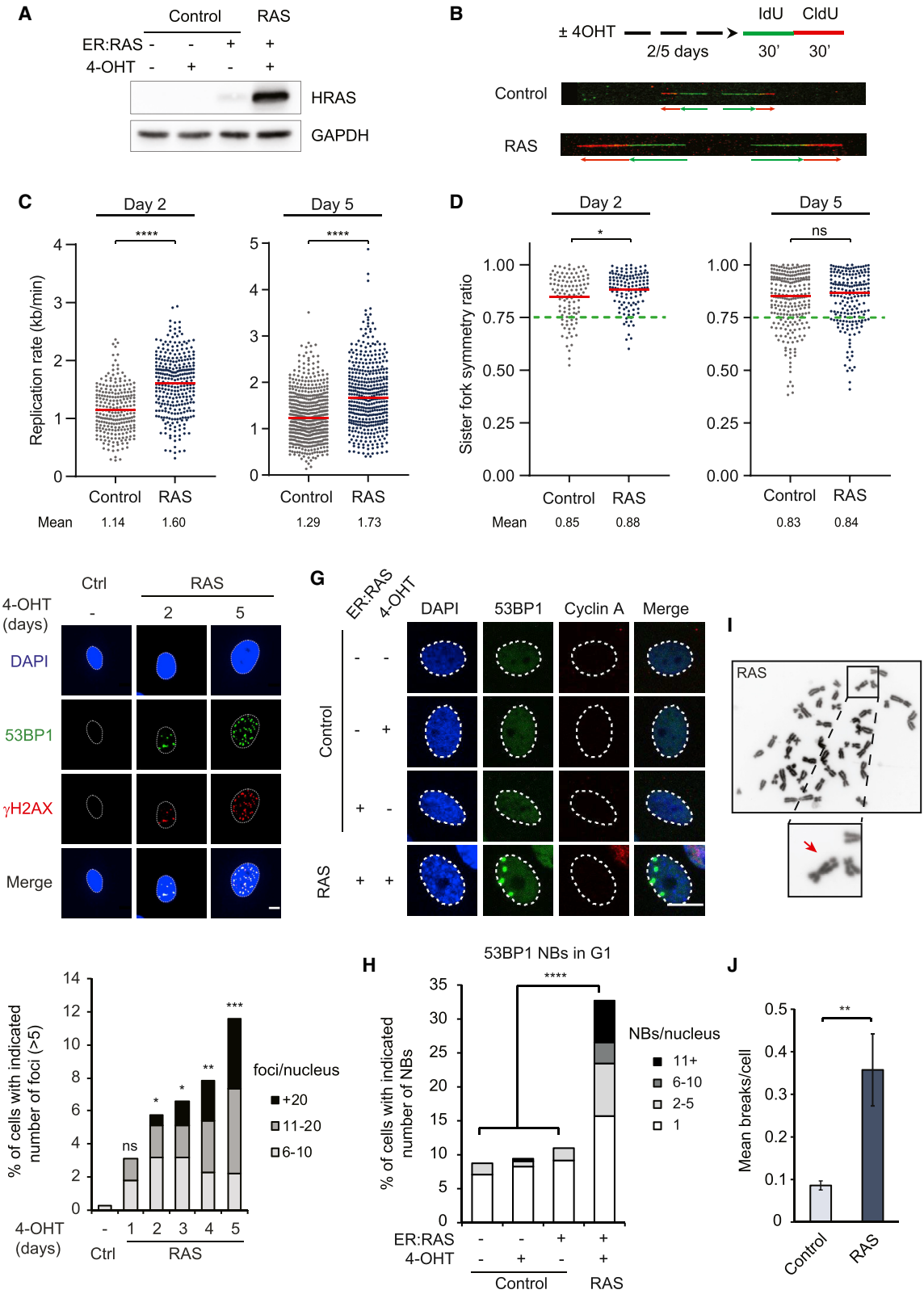

(legend on next page)

accelerates DNA replication and generates DNA damage. These results highlight the important role of TOP1 in maintaining genome stability by controlling R-loop homeostasis, enabling tight regulation of DNA replication fork progression. Additionally, high TOP1 expression in tumors is associated with replication-induced mutations, suggesting that TOP1-induced accelerated replication may promote mutagenesis. Altogether, the results of our study reveal a novel mechanism of oncogene-induced DNA damage induced by aberrant replication fork acceleration.

RESULTS

RAS expression induces replication acceleration in pre-senescent cells

RAS proteins (HRAS, KRAS, NRAS) are members of a GTP-binding protein family (Pylayeva-Gupta et al., 2011), regulating numerous cellular processes including cell-cycle progression (Downward, 2003). Mutated RAS expression induces genomic instability leading to senescence, an antitumor cell-cycle arrest state (Denko et al., 1994; Saavedra et al., 2000; Yang et al., 2013). However, cells escaping this proliferation inhibition drive tumorigenesis (Halazonetis et al., 2008). Therefore, we first investigated the effect of RAS on DNA replication dynamics in pre-senescent cells. For this, immortalized human foreskin fibroblasts were retrovirally infected with an inducible ER:HRAS-G12V vector (RAS). RAS selective expression following 4-hydroxytamoxifen (4-OHT) supplementation was verified by western blot (Figures 1A and S1A). Following RAS activation, cells entered a hyperproliferative phase, as indicated by increased population doubling and IdU incorporation already at day 2 (Figures S1B–S1D). This was followed by a decline in the proliferative potential until proliferation ceased by day 10, when cells entered senescence, as indicated by reduced population doublings, reduced IdU incorporation, and increased senescence associated β-gal activity (Figures S1B–S1F). Hence, the effect of RAS activation on replication dynamics and genome stability was investigated in pre-senescence RAS-expressing cells up to 5 days following RAS induction.

We then analyzed the effect of RAS activation on replication dynamics using DNA combing, which enables replication analysis of single DNA molecules (Figure 1B). The analysis showed a remarkable increase in the mean replication rate on both days 2 and 5, following RAS activation (Figure 1C). Similar results were obtained in another cell line of fetal human lung fibroblasts, WI-38 (Figures S1G and S1I).

Previous studies have shown that slowed replication is correlated with an increased number of activated origins (Courbet et al., 2008; Ge et al., 2007). Therefore, we investigated origin activation in RAS-expressing cells. Analysis of the mean replication fork distance showed a significant increase on both days 2 and day 5 following RAS activation (Figure S1H). Similar results were obtained in WI-38 cells (Figure S1J). These results indicate that in pre-senescent RAS-expressing cells, there was a significant increase in the rate of replication along with a decrease in local origin activation.

Fork stalling induced by replication stress manifests as asymmetrical progression of sister forks emanating from the same origin (Conti et al., 2007). In order to further characterize the accelerated replication rate following RAS expression, we compared the progression of left and right outgoing sister replication forks. The analysis showed no significant decrease in fork symmetry following RAS expression on both days 2 and 5 compared with control cells (Figure 1D), indicating no increase in fork stalling. Similar results were obtained in WI-38 cells (Figure S1K). Altogether, these results indicate a non-classical form of aberrant replication dynamics in pre-senescent RAS-expressing cells, exhibited by accelerated replication and decreased origin activation. This aberrant acceleration was observed both in the hyperproliferative phase (day 2) and shortly before cells senesce (day 5).

RAS leads to accelerated replication-induced DNA damage

Slow replication rate, induced by oncogenes, including mutated RAS OE, generates DNA damage and activates damage response pathways (Abulaiti et al., 2006; Aird et al., 2013; Kotsantis et al., 2016; Macheret and Halazonetis, 2015). In order to determine whether RAS-induced fork acceleration causes DNA damage, we examined cellular DNA damage response markers known also to be induced under replication stress (Ewald et al., 2007). We first analyzed DNA damage by co-localization of phosphorylated H2AX (γH2AX) and 53BP1 foci. The

Figure 1. RAS expression leads to increased replication rate and DNA damage

(A) Protein levels of HRAS and GAPDH in FSE-hTert cells with (+) or without (−) ER:RAS infection and 5 day 4-OHT treatment, as indicated.

(B) Scheme of the protocol and exemplary images of DNA combing.

(C) Fork rate (kb/min) in control and RAS-expressing cells for 2 or 5 days; at least 240 fibers per condition were analyzed.

(D) Sister fork symmetry in control and RAS-expressing cells for 2 or 5 days; at least 100 fibers per condition were analyzed. Dashed green line indicates asymmetry ratio threshold.

(C and D) Red lines indicate medians, and means are indicated. Data for RAS day 2 are the summary of 2 independent experiments; data for RAS day 5 are the summary of 4 independent experiments. Mann-Whitney rank-sum test.

(E and F) Co-localization of γH2AX (red) and 53BP1 (green) foci in control and RAS-expressing cells for the indicated time points (days). Representative images (E), and percentage of cells with indicated number of co-localized γH2AX and 53BP1 foci per nucleus (F); at least 380 nuclei per condition were analyzed. Data are the summary of three independent experiments. p values were calculated compared with control (Ctrl) by one-way ANOVA.

(G and H) 53BP1 NBs (green) in G1-phase (cyclin A negative, red) cells, as indicated in (A). Representative images (G), and percentage of cells with indicated number of NBs per nucleus (H); at least 85 nuclei per condition were analyzed. Only NBs >1 μm in diameter were scored. p values were calculated compared with RAS. Data are representative of three independent experiments with similar results.

(I) An exemplary image of a metaphase spread in RAS cells; red arrow indicates a break.

(J) Quantification of chromosomal aberrations detected in metaphase spreads of RAS cells (n = 120) or Ctrl cells (n = 155). Data are from two independent experiments, and means ± SEM are shown. ns, non-significant; *p < 0.05, **p < 0.01, ***p < 0.001, ****p < 0.0001. Scale bars, 10 μm.

analysis showed a significant increase in DNA damage already on day 2 post RAS activation (Figures 1E and 1F), when aberrant accelerated replication is already found (Figure 1C). Interestingly, the levels of DNA damage markers increased in these cells over time (Figures 1E and 1F), implying that the accumulation of unrepaired damage may lead to cell-cycle arrest (Bartkova et al., 2006; Halazonetis et al., 2008; Di Micco et al., 2006). Next, we investigated whether the observed damage is associated with replication stress, known to induce DNA lesions that manifest as nuclear bodies (NBs) of 53BP1 in the G1 phase of the next cell cycle (Lukas et al., 2011). Analysis of 53BP1 NBs (>1 μm in diameter) in G1-phase cells (cyclin A negative) showed a significant increase in NB formation in RAS-expressing cells compared with control cells (Figures 1G and 1H). In contrast to large 53BP1 NBs, small 53BP1 foci were reported to form at double-strand breaks (DBSs) irrespectively of replication stress (Palmerola et al., 2022; Schultz et al., 2000). Interestingly, analysis of small 53BP1 foci (<1 μm in diameter) in G1 cells showed an increase in foci formation in RAS-expressing cells (Figures S2A and S2B), suggesting that RAS induced both replicative and non-replicative DNA damage. Furthermore, we found in RAS-expressing cells a significant increase in γH2AX, a DNA damage marker also induced upon replication stress (Figures S2C and S2D) (Ewald et al., 2007). Next, we analyzed whether RAS activation leads to the expression of fragile sites, hotspots of genomic instability. These sites are sensitive to replication stress conditions, as they fail to complete DNA replication, leaving underreplicated regions that manifest as chromosomal breaks in metaphase chromosomes (Glover et al., 1984; Miron et al., 2015). Metaphase spread analysis showed a significant increase in chromosomal fragility in RAS-expressing cells (Figures 1I and 1J), implying that the replication perturbation induced by RAS generates replication-induced genomic instability. We then tested CHK1 phosphorylation, a hallmark of the replication stress response (Zeman and Cimprich, 2014). A significant increase in CHK1 phosphorylation was found in RAS-expressing cells (Figures S2E and S2F). Overall, these results suggest that the RAS-induced DNA damage is associated with aberrant acceleration of DNA replication.

Reducing the accelerated replication fork progression rescues the DNA damage phenotype

We next investigated whether accelerated replication could be the cause for DNA damage in RAS-expressing pre-senescent cells. For this, we treated RAS-cells with hydroxyurea (HU), an inhibitor of replication fork progression, to slow the accelerated replication and analyzed its effect on DNA damage. HU inhibits the ribonucleotide reductase (RNR), thus reducing the deoxyribonucleotide pool, resulting in reduced replication rates in a dose-dependent manner (Ge and Blow, 2010; Skoog and Nordenskjöld, 1971; Técher et al., 2016). Whereas high doses of HU (≥1 mM) lead to fork arrest, low doses (≤0.1 mM) decelerate replication fork rate (Koundrioukoff et al., 2013; Técher et al., 2016). Therefore, we used relatively low HU concentrations and analyzed their effect on the replication dynamics. Cells expressing RAS for 5 days were treated with 0.001–0.1 mM HU for 48 h prior to the analysis, which allowed the cells to go through at least one cell cycle under inhibitory conditions (Figure 2A). Flow cytometry analysis showed no significant change in the cell-cycle progression, indicating that HU treatment did not arrest cell proliferation (Figures S3A and S3B). DNA combing analysis revealed that mild replication inhibition of RAS cells with 0.01 mM HU resulted in a dramatic fork deceleration compared with non-treated RAS cells (Figure 2B). The mean rate in these HU-treated RAS cells showed no significant difference compared with control cells, indicating restoration of replication fork rate (Figure 2B). This HU concentration also led to a reduction in the fork distance in RAS-expressing cells to the normal distance observed in the control cells (Figure 2C). Finally, 0.01 mM HU treatment did not induce sister fork asymmetry in RAS-expressing cells, indicating that this low HU concentration did not induce fork stalling (Figure 2D). These results indicate that mild replication inhibition in RAS-expressing cells rescued the perturbed DNA replication, resulting in the restoration of normal replication dynamics.

Next, we investigated whether the replication rate restoration affected RAS-induced DNA damage. For this, cells were treated with 0.01 mM HU for 48 h prior to DNA damage analysis by immunofluorescence detection of co-localized γH2AX and 53BP1 foci. Mild HU treatment in control cells did not lead to DNA damage induction (Figure S3C). However, 0.01 mM HU treatment led to a significant decrease in the number of RAS-induced damage foci compared with non-treated RAS-expressing cells (Figures 2E and 2F). It is worth noting that the highest HU concentration (0.1 mM) used decreased dramatically the replication rate even when compared with control cells (Figure 2B) and led to increased DNA damage compared with non-treated RAS-expressing cells (Figures 2E and 2F). A considerably lower dose of HU (0.001 mM) had a limited, non-significant effect on the replication rate (Figure 2B) and, as expected, had no significant effect on DNA damage formation compared with RAS-expressing cells not treated with HU (Figures 2E and 2F). Altogether these results indicate that restoration of the accelerated replication rate dramatically reduced the DNA damage in RAS-expressing cells.

We further investigated the effect of replication restoration on DNA damage by examining the effect of aphidicolin (APH), another replication inhibitor, which inhibits DNA polymerases α, δ, and ε and decreases fork progression in a dose-dependent manner (Cheng and Kuchta, 1993; Ikegami et al., 1978). RAS-expressing cells were treated with relatively low APH concentrations for 48 h prior to replication dynamics and DNA damage analyses. Flow cytometry analysis showed no significant change in cell-cycle progression, indicating that like HU, APH treatment did not arrest cell proliferation (Figures S3A and S3B). Co-localization analysis of γH2AX and 53BP1 foci revealed that a low dose of 0.01 μM APH significantly decreased the number of damage foci in RAS-expressing cells compared with non-treated RAS cells (Figures S3D and S3E), while it had no effect on the level of the damage markers in control cells (Figure S3C). Furthermore, similar to the effect of various HU concentrations, a very low dose of APH (0.001 μM) did not have a significant effect on DNA damage in RAS-expressing cells compared with non-treated RAS-expressing cells (Figure S3E); by contrast, a high dose of 0.1 μM APH induced DNA damage (Figure S3E). Finally, we investigated whether the DNA damage rescue by

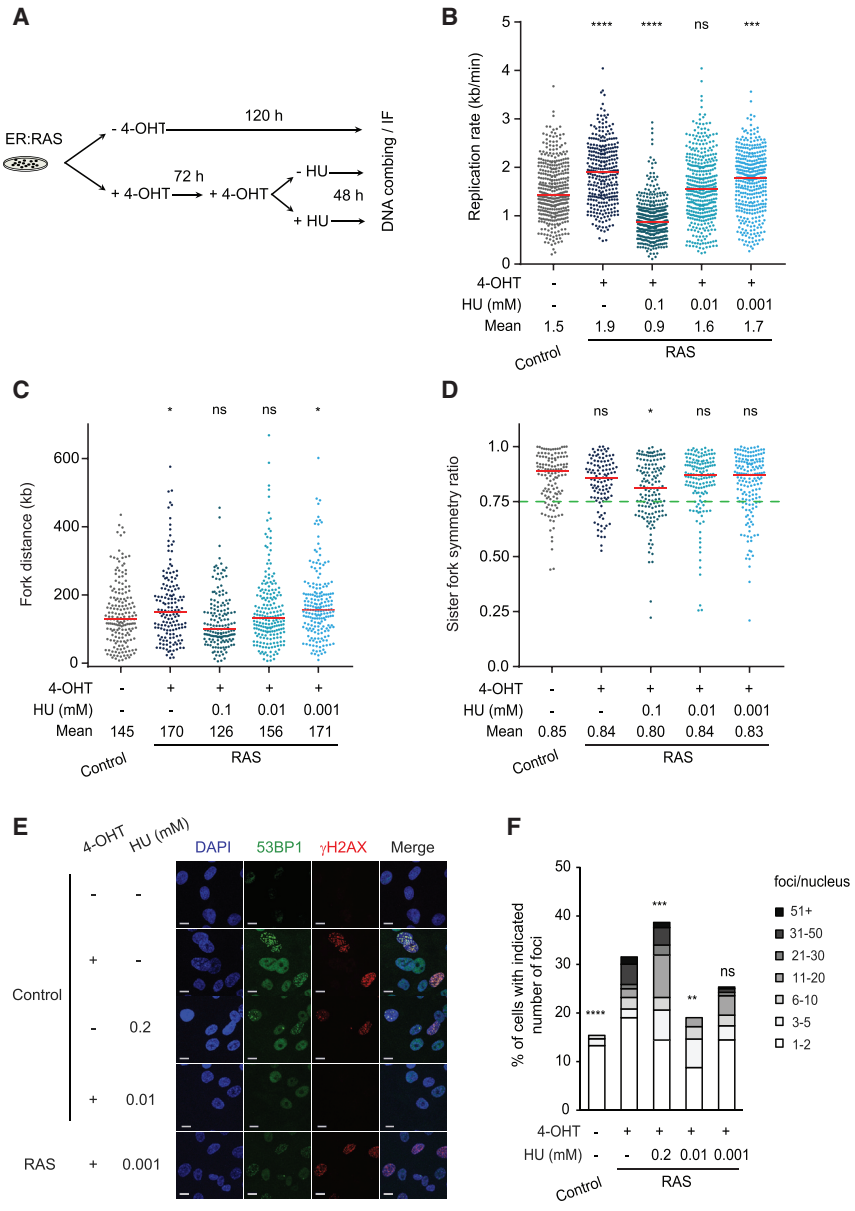

Figure 2. Mild replication inhibition restores normal replication dynamics and rescues DNA damage

(A) Scheme of the protocol. Replication and damage analysis in RAS cells ± HU treatment, as indicated. (B–D) DNA combing analysis of Ctrl and RAS cells ± HU treatment, as indicated. (B) Fork rate (kb/min); at least 300 fibers per condition were analyzed. (C) Fork distance (kb); at least 150 forks per condition were analyzed. (D) Sister fork symmetry; at least 110 forks per condition were analyzed. Means are indicated, and red lines indicate medians. p values were calculated compared with Ctrl by one-way ANOVA. Data are the summary of two independent experiments. (D) Dashed green line indicates asymmetry ratio threshold.

(E and F) Co-localization of γH2AX (red) and 53BP1 (green) foci, as indicated in (B). Representative images (E), and percentage of cells with indicated number of foci per nucleus (F); at least 190 nuclei per condition were analyzed. Data are representative of two independent experiments with similar results. p values were calculated compared with RAS cells by Mann Whitney rank-sum test. ns, non-significant; *p < 0.05, **p < 0.01, ***p < 0.001, ****p < 0.0001. Scale bars, 10 μm.

the 0.01 μM APH treatment was associated with replication restoration. As expected, DNA combing analysis showed restoration of the replication dynamics by the APH treatment (Figures S3F–S3H), altogether suggesting that accelerated replication generates DNA damage.

Excess TOP1 causes accelerated replication rate and DNA damage in RAS-expressing cells

To explore the molecular mechanism/s underlying the accelerated replication in RAS cells, we examined the differences in gene expression after mutated RAS activation. For this, we performed RNA sequencing (RNA-seq) analysis on control and RAS-expressing cells at two time points, at 2 and 4 days post RAS activation, when cells are proliferating. Principal-component analysis showed that the expression profiles of RAS cells clustered together and were distinguishable from control cells (Figure S4A). After RAS activation, >1,700 genes were differentially expressed, with an estimated false discovery rate (FDR) of <5% and a fold change >2-fold (Figure S4B). Gene Ontology (GO) annotation analysis of the upregulated genes following RAS activation (shared at both time points, 282 genes) showed enrichment for signaling and developmental processes (Figure S4C). Among the shared downregulated genes (568 genes) in RAS cells, GO annotation analysis identified enrichment of anatomical and developmental processes (Figure S4C). DNA replication was not found among the GO annotations significantly enriched after RAS activation. Therefore, we next focused on individual DNA replication annotated genes (GO: 0006260) to identify specific differentially expressed genes in RAS compared with control cells, which could lead to dysregulation of the replication process. Previously, deregulation of origin firing factors such as *CDC7*, *ORC1*, *MCM4*, *MCM6*, *Treslin*, and *MTBP* have been shown to lead to an increased replication rate in various organisms (Flach et al., 2014; Maya-Mendoza et al., 2018; Sedlackova et al., 2020; Zhong et al., 2013). However, our analysis showed no significant change in the expression level of any of these genes or other origin licensing or firing genes (Figure 3A; Table S1), suggesting that in our system, the accelerated replication rate was not the result of a decreased origin usage.

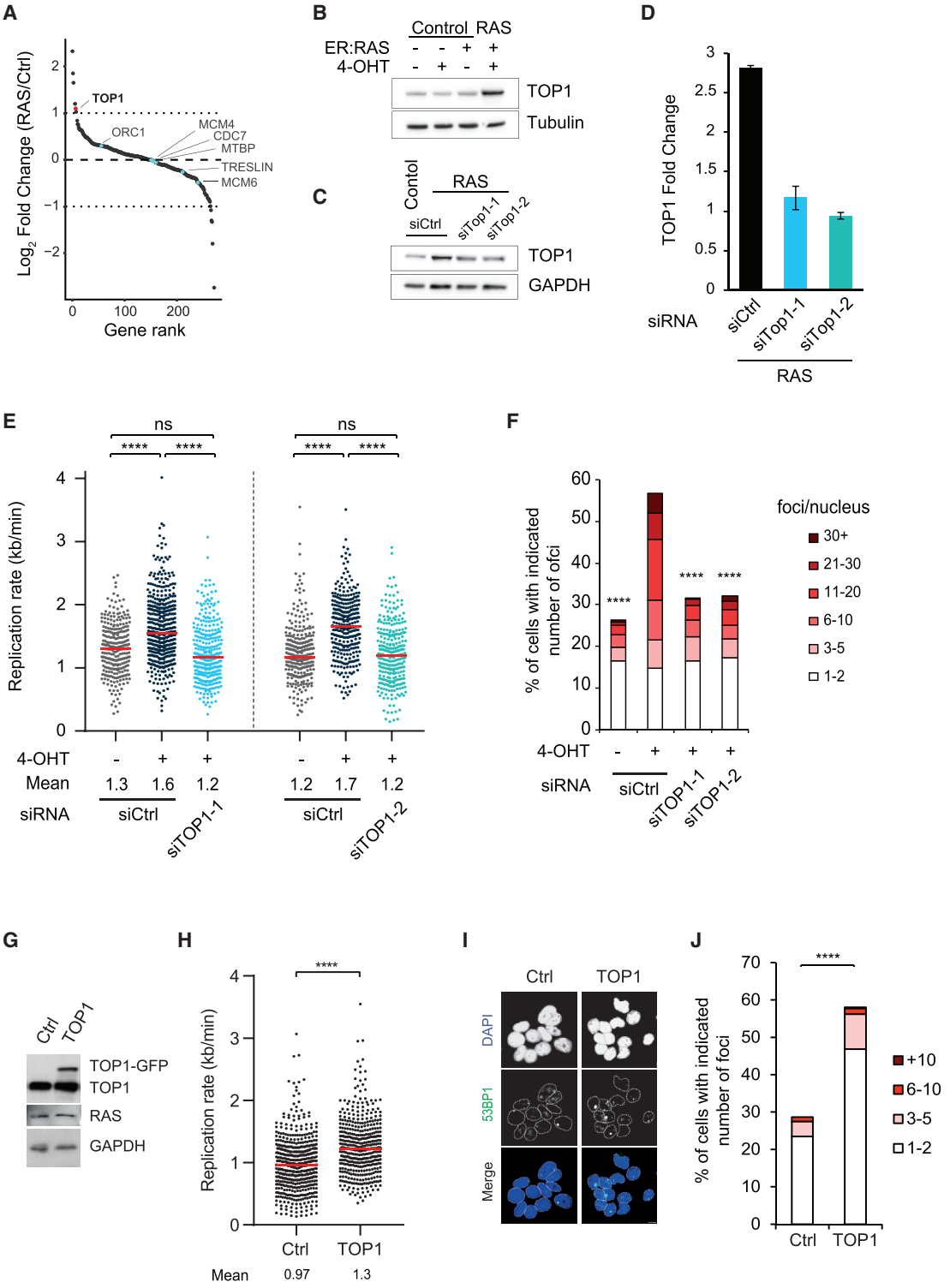

Figure 3. Increased TOP1 expression causes accelerated DNA replication and DNA damage

(A) Expressed DNA replication annotated genes (GO: 0006260, n = 258) ranked according to the RAS/Ctrl fold change. Light blue, genes previously associated with accelerated replication; red, TOP1.

(B) Protein levels of TOP1 and Tubulin in Ctrl and RAS cells, as indicated.

(legend continued on next page)

Analysis of replication annotated genes identified only five genes upregulated by at least 2-fold following RAS activation: *E2F7*, *EREG*, *EGFR*, *HMGA1*, and *TOP1* (Figures 3A; Table S1). Interestingly, TOP1 downregulation was reported to reduce replication fork rate and induce DNA damage (Promonet et al., 2020; Tuduri et al., 2009). TOP1 is an essential protein in mammalian cells that resolves DNA torsional stress induced during replication and transcription (Pommier, 2006; Pommier et al., 2016). Therefore, we set to investigate the role of elevated TOP1 in regulation of accelerated DNA replication. First, we validated the increased level of TOP1 in RAS cells by western blot and qRT-PCR (Figures 3B and S5A). We then explored the relevance of TOP1 OE for cancer. Analysis of The Cancer Genome Atlas (TCGA) datasets revealed a 2-fold increase in TOP1 in 9/33 cancer types, as found in our RAS-induced system (Figure S5B). Interestingly, the expression of NRAS is also significantly increased in all 9 cancer types (Figure S5B). We further identified that TOP1 and NRAS expression was positively correlated in 8/9 cancer types (Figure S5C), further supporting the possible link between RAS activation and TOP1 OE. It is worth noting that in cancers, the expression of each RAS family gene member is not necessarily correlated with each other, potentially due to their redundant function (Stephens et al., 2017). Indeed, our TCGA analysis showed no significant change in the expression of KRAS or HRAS in most of the 9 cancer types in which TOP1 and NRAS are increased (Figure S5B), thus suggesting that each RAS member may increase TOP1 expression.

We then looked for possible transcription factors that can bind the promoter of TOP1 and contribute to its increased expression in four separate transcription factor binding databases, ChIP Enrichment Analysis (CHEA), Encyclopedia of DNA Elements (ENCODE), MotipMap, and TRANSFAC, and found one transcription factor shared between all four databases, MYC (Figure S5D; Table S2). Interestingly, the expression of MYC is significantly increased in 7/9 TCGA cancer types in which TOP1 is increased (Figure S5B). Accordingly, in our RAS-expressing cells MYC was overexpressed compared with control cells (Figure S5E). These results are in agreement with previous studies showing that RAS upregulates the expression of MYC (Kerkhoff et al., 1998) and enhances MYC protein stability (Sears et al., 1999). Furthermore, a recent report found that MYC recruits TOP1 to actively transcribed genes and stimulates its activity (Das et al., 2022), thus supporting the hypothesis that OE of RAS increases the expression and activity of MYC, which subsequently contributes to the activation of TOP1 transcription and to its activity at transcribed genes.

To explore the effect of excess TOP1 levels on replication dynamics and DNA damage, we first restored normal TOP1 level in RAS-expressing cells by moderate downregulation of TOP1 using low concentrations of two independent small interfering RNAs (siRNAs) (Figures 3C and 3D). We then examined the effect of TOP1 restoration on replication dynamics. The analysis showed that TOP1 restoration significantly reduced the replication rate in siTOP1-treated RAS-expressing cells compared with control siRNA-treated RAS cells (Figure 3E), which was indistinguishable from the rate of the control cells, indicating complete restoration of a normal replication rate (Figure 3E). TOP1 restoration also significantly reduced the fork distance in siTOP1-treated RAS cells compared with control siRNA-treated RAS cells (Figure S6A), indicating restoration of the replication dynamics. Finally, TOP1 restoration did not affect sister fork symmetry (Figure S6B). Downregulation of TOP1 in control cells using the same low concentrations of siTOP1 led to significant reduction in replication rate and fork distance compared with treatment with a control siRNA (Figures S6C–S6E), in agreement with previous results (Promonet et al., 2020; Tuduri et al., 2009). Furthermore, downregulation of TOP1 in control cells significantly reduced the sister forks symmetry ratio (Figure S6F) and increased DNA damage (Figure S6G), suggesting that deficit in TOP1 leads to classical replication stress, whereas excess TOP1 drives a non-canonical form of replication stress characterized by fork acceleration.

We further investigated the effect of TOP1 restoration on RAS-induced DNA damage. Analysis of γH2AX foci showed a significant decrease in damage foci following TOP1 downregulation in RAS cells compared with control siRNA-treated RAS cells (Figure 3F), indicating that restoration of TOP1 to the normal level of control cells rescues DNA damage. Altogether, these results suggest that regulated TOP expression1 is crucial since both increased and decreased TOP1 levels are deleterious to cells.

Reduced TOP1-dependent R-loops promote accelerated replication and DNA damage

To test our hypothesis that excess TOP1 accelerates replication rate leading to DNA damage, we overexpressed TOP1 in HEK-293 cells, in which RAS expression was not affected (Figure 3G), and analyzed its effect on replication dynamics. TOP1 OE significantly increased the mean replication rate (Figure 3H) and, accordingly, increased the fork distance (Figure S6H). Fork

(C) Protein levels of TOP1 and GAPDH in Ctrl and RAS cells treated with two independent siRNAs against TOP1 (siTOP1-1 and siTOP1-2) or non-targeting siRNA (siCtrl), as indicated.
(D) qRT-PCR of TOP1 normalized to GAPDH in RAS cells treated with siTOP1, as indicated. The values are averaged fold change (mean ± SEM, n = 2) relative to Ctrl (non-RAS) cells treated with siCtrl.
(E) Fork rate (kb/min) of cells, as indicated in (C); at least 270 fibers per condition were analyzed. Means are indicated, and red lines indicate medians. p values were calculated by one-way ANOVA. Data are the summary of two independent experiments.
(F) Percentage of cells with the indicated number of γH2AX foci in cells, as indicated in (C); at least 1,000 nuclei per condition were analyzed. p values were calculated compared with siCtrl RAS cells. Data are representative of three independent experiments.
(G) Protein levels of endogenous TOP1 (TOP1), ectopic TOP1 (TOP1-GFP), RAS, and GAPDH in HEK-293 cells transfected with a control GFP vector (Ctrl) or with TOP1-GFP (TOP1), as indicated.
(H) Fork rate (kb/min) of HEK-293 cells, as indicated in (G); at least 400 fibers per condition were analyzed.
(I and J) 53BP1 (green) foci in HEK-293 cells, as indicated in (G). Representative images (I). Percentage of cells with indicated number of foci (J). At least 300 nuclei were analyzed. Data are representative of two independent experiments. ns, non-significant; ****$p < 0.0001$. Scale bars, 10 μm.

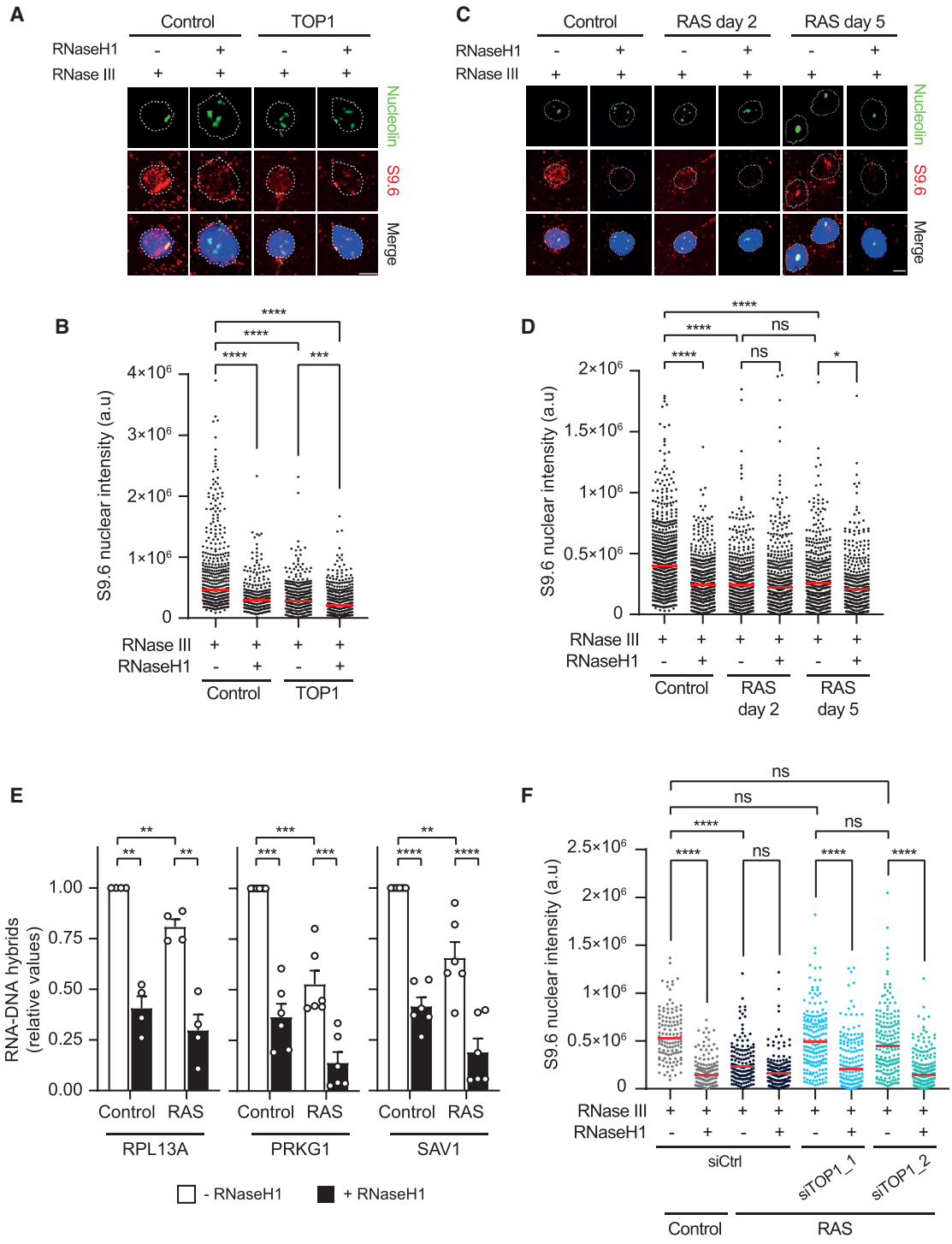

Figure 4. Elevated TOP1 reduces R-loop accumulation

(A and B) RNA-DNA hybrids in HEK-293 cells transfected with a control GFP vector (Ctrl) or with TOP1-GFP (TOP1), treated with (+) RNase III and with (+) or without (–) RNaseH1, as indicated. Representative images of RNA-DNA antibody (S9.6, red), nucleolin (green), and DAPI (blue) staining (A). Mean nuclear fluorescence intensity of RNA-DNA hybrid antibody (S9.6) after nucleolar signal removal (B). At least 600 nuclei were analyzed. Data are summary of two independent experiments.

(C and D) RNA-DNA hybrids in ER:RAS FSE hTert cells with (RAS) or without (Ctrl) 4-OHT treatment treated with RNaseIII and RNaseH1, as indicated. Representative images, staining as in (A) (C). Mean nuclear fluorescence intensity of RNA-DNA hybrids (S9.6 antibody) after nucleolar signal removal in Ctrl and RAS-expressing cells for 2 or 5 days (D).

(legend continued on next page)

symmetry analysis revealed no increase in asymmetric fork progression following TOP1 OE (Figure S6I), indicating that excess TOP1 expression accelerated DNA replication without causing fork stalling. Next, we measured 53BP1 foci levels in TOP1-overexpressing cells. The analysis showed an increase in the mean number of foci following TOP1 OE compared with control cells (Figures 3I and 3J), supporting our findings that TOP1-dependent accelerated replication leads to DNA damage.

We hypothesize that elevated TOP1 could promote accelerated replication by reducing the abundance of R-loops and therefore decrease potential obstacles to the replication machinery. R-loops are RNA-DNA hybrids formed during transcription, and their aberrant accumulation may stall replication fork progression and lead to DNA damage (Santos-Pereira and Aguilera, 2015). Negative supercoiling, formed behind the transcribing RNA polymerase, promotes DNA strand separation, which increases the possibility of the nascent transcript to anneal to the DNA and form an R-loop (Santos-Pereira and Aguilera, 2015). TOP1 relieves the negative supercoiled DNA and thus prevents R-loop formation (Santos-Pereira and Aguilera, 2015). Indeed, TOP1 inhibition/downregulation increases the R-loop level (Promonet et al., 2020; Tuduri et al., 2009). Therefore, we investigated the effect of increased TOP1 on R-loop accumulation. We used the S9.6 antibody to detect RNA-DNA hybrids in control and TOP1-overexpressing cells. To ensure that the S9.6 antibody identifies only RNA-DNA hybrids, cells were treated with RNase III, which cleaves double-stranded RNA (dsRNA) that might be detected by the S9.6 antibody. Immunofluorescence analysis indeed showed a significant decrease in the S9.6 nuclear staining in TOP1-overexpressing cells compared with control cells (Figures 4A and 4B). Treatment with RNaseH1, which degrades the RNA transcript of an RNA-DNA hybrid, showed a significant decrease in nuclear S9.6 staining, conforming the specific detection of R-loops. Thus, increased TOP1 led to a reduction in R-loops.

Next, we explored the effect of excess TOP1 on R-loop levels in RAS-expressing cells. Analysis of RNA-DNA hybrid levels showed a significant decrease in R-loops in RAS-expressing cells for 2 and 5 days compared with control cells (Figures 4C and 4D). We further performed DNA-RNA hybrid immunoprecipitation (DRIP) analysis to study R-loop accumulation at specific transcribed genes: *RPL13A*, *PRKG1*, and *SAV1*. The results showed a significant decrease in RNA-DNA hybrids, in RAS cells, consistent with the immunofluorescence results (Figure 4E). Treatment with RNaseH1 showed a significant decrease in the DRIP values, confirming the specific detection of RNA-DNA hybrids (Figure 4E). Altogether, the RNA-DNA hybrid analyses show reduced R-loop levels in RAS-expressing cells.

We then analyzed the effect of TOP1 restoration in RAS cells on R-loops using two independent siRNAs against TOP1. The results showed that the siTOP1 treatment increased R-loop levels in RAS-expressing cells back to normal levels of control cells (Figure 4F). These results indicate that TOP1 restoration in RAS cells restores R-loop levels and rescues the accelerated replication rate. Similarly, mild replication inhibition by HU/APH, which restored normal replication dynamics (Figures 2 and S3), also increased R-loop levels back to normal, without affecting the TOP1 level (Figures S6J and S6K). Altogether, these results suggest that R-loop restoration rescues the perturbed DNA replication.

To further explore the direct effect of R-loop suppression on replication dynamics, we overexpressed RNaseH1 in HEK-293 cells (Figure 5A). RNaseH1 OE reduced R-loop levels compared with control cells (Figures 5B and 5C) and significantly accelerated the replication rate (Figure 5D). Accordingly, RNase H1 OE increased the mean fork distance Figure 5E). Fork symmetry analysis revealed no change following RNaseH1 OE (Figure 5F). Lastly, immunofluorescence analysis of 53BP1 foci showed an increase in the mean number of foci following RNaseH1 OE compared with control cells (Figures 5G and 5H). Taken together, these results indicate that suppressed R-loop levels promote replication fork acceleration and lead to the formation of DNA damage.

Restored replication in SRSF1-deficient RAS cells

TOP1-induced accelerated replication might result from R-loop dysregulation (Figures 4 and 5) or from TOP1 relaxation of supercoiled DNA ahead of the replication fork. To distinguish between these two possibilities, we investigated the replication dynamics under normal R-loop levels in RAS-expressing cells in a TOP1-independent manner. For this, we downregulated the splicing factor SRSF1, shown to increase R-loop accumulation without interfering with the relaxation of supercoiled DNA (Li and Manley, 2005; Promonet et al., 2020). SRSF1 downregulation by siRNA normalized R-loop levels in RAS-expressing cells (Figures 6A and 6B). Analysis of the replication dynamics in the siSRSF1-treated RAS cells showed normalized replication rate (Figure 6C) and fork distance (Figure 6D), with no significant effect on sister fork symmetry (Figure 6E). Moreover, siSRSF1 treatment resulted in a significant decrease in DNA damage in RAS-expressing cells (Figures 6F and 6G). Altogether, these results suggest that TOP1-induced accelerated replication is caused by R-loop dysregulation and not by excess relaxation of supercoiled DNA.

High TOP1 is associated with DNA replication mutagenesis

The mechanisms underlying DNA damage induced by replication fork slowing/stalling have been widely investigated (Gaillard et al., 2015; Zeman and Cimprich, 2014). However, little is known about how accelerated replication promotes DNA damage. Previously, we showed that oncogene-induced classical replication stress results from enforced cell proliferation under insufficient

(E) DRIP-qPCR using S9.6 antibody in Ctrl and RAS-expressing cells for 2 days, at RPL13A, PRKG1, and SAV1 genes. Independent replicates are presented as circles. Mean ± SEM. p values were calculated by Student's t test.

(F) Mean nuclear fluorescence intensity of RNA-DNA hybrid antibody (S9.6) after nucleolar signal removal in Ctrl and RAS cells treated with siRNA, RNaseIII, and RNaseH1, as indicated.

(B, D, and F) Red lines indicate medians, p values were calculated by one-way ANOVA ns, non-significant; *p < 0.05; **p < 0.01; ***p < 0.001, ****p < 0.0001. Scale bars, 10 μm.

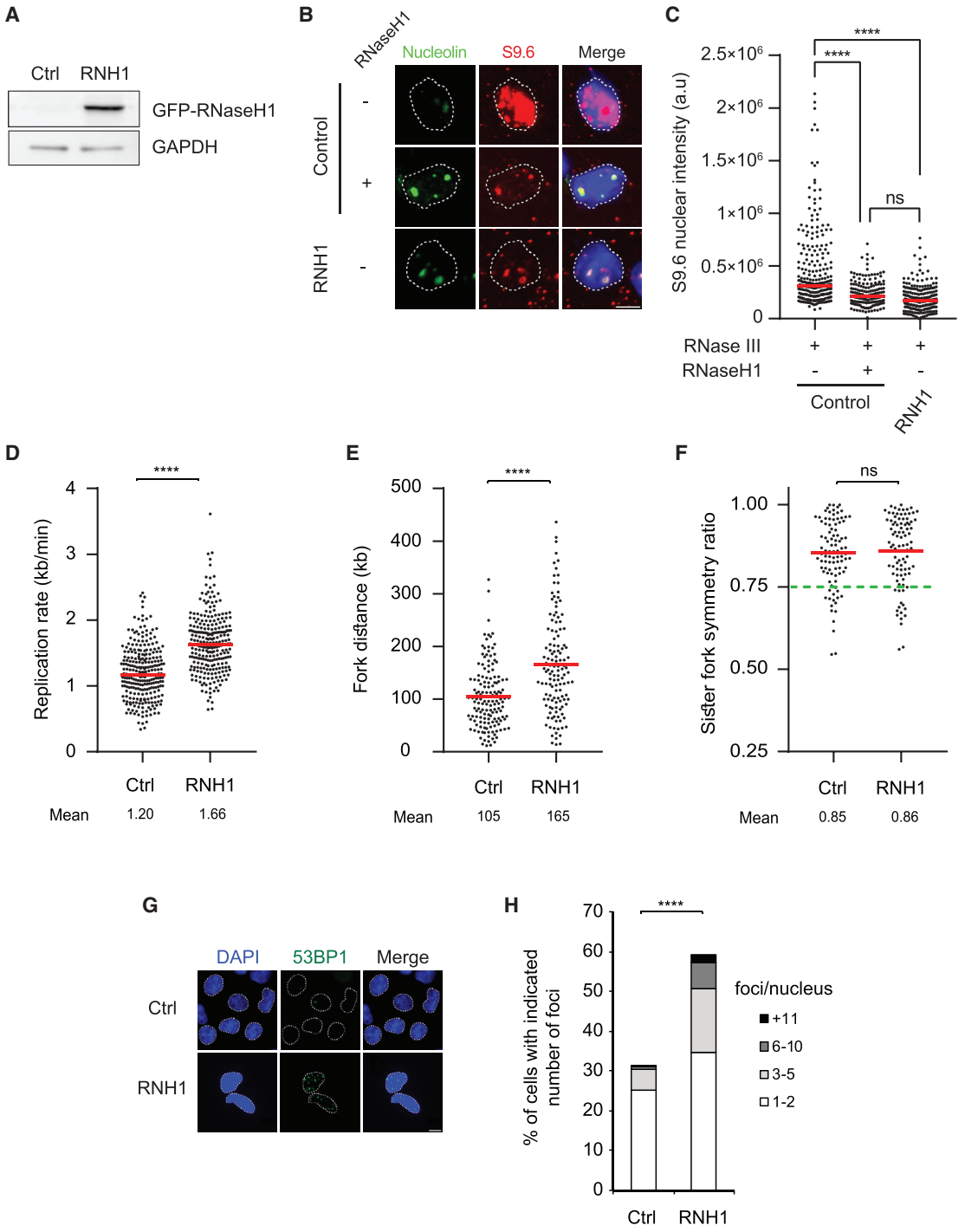

Figure 5. Reduced R-loops cause accelerated DNA replication rate and DNA damage

(A) Protein levels of GFP-RNaseH1 and GAPDH in HEK-293 cells transfected with a Ctrl GFP plasmid (Ctrl) or with GFP-RNaseH1 plasmid (RNH1).

(B and C) RNA-DNA hybrids in Ctrl and RNaseH1 cells (RNH1). Representative images of RNA-DNA antibody (S9.6, red), nucleolin (green), and DAPI (blue) staining (B). Mean nuclear fluorescence intensity of RNA-DNA hybrid antibody (S9.6) after nucleolar signal removal of Ctrl and RNaseH1 cells, treated with RNase III and RNaseH1, as indicated (C). At least 300 nuclei were analyzed. Data are the summary of two independent experiments. Red lines indicate medians p values were calculated by one-way ANOVA.

(legend continued on next page)

nucleotide biosynthesis to support normal replication (Bester et al., 2011). Therefore, we investigated whether the DNA damage following RAS-induced accelerated replication could result from a nucleotide deficiency. We analyzed 53BP1 NBs and foci in the G1 phase in RAS-expressing cells grown in a regular medium or in a medium supplemented with exogenous nucleosides. The analysis showed no significant difference in 53BP1 NBs or foci (Figures S7A–S7C), indicating that DNA damage in these cells with accelerated replication was not the result of nucleotide insufficiency.

TOP1 cleavage complexes (TOP1ccs) trapped on the DNA can promote DNA lesions (Pommier et al., 2006). Hence, we tested whether excess TOP1 may lead to an overload of TOP1ccs that could directly lead to DNA damage. To do so, we overexpressed TDP1, which removes TOP1ccs from the DNA (Pommier et al., 2006), in HEK-293 TOP1-overexpressing cells (Figure S7D). DNA damage analysis of 53BP1 foci showed no significant difference between TDP1-overexpressing cells and control cells (Figure S7E), indicating that the DNA damage formed in TOP1-overexpressing cells is not the result of excess TOP1ccs covalently linked to the DNA. We then further explored whether high levels of TOP1 would sensitize oncogenic cells to TOP1cc-generating agents, which could be used as therapy for patients with cancer. For this, we treated RAS-expressing cells with increasing concentrations of the TOP1 inhibitor camptothecin (CPT) (Pommier, 2006). Cell viability assay showed that RAS cells were indeed more sensitive to CPT treatment compared with control cells (Figure S7F). Next, we normalized TOP1 expression in RAS cells using siRNAs and tested their response to CPT. The results showed that in RAS-expressing cells, TOP1 restoration had no significant effect on cell viability compared with RAS cells treated with a control siRNA (Figure S7F). Thus, in these RAS-expressing cells, the elevated TOP1 expression did not sensitize cells to CPT.

Ribonucleotides are incorporated into the DNA during replication and are safely removed by the ribonucleotide excision repair (RER) pathway. However, in RER-deficient cells ,incorporated ribonucleotides are cleaved by TOP1 in a process that leads to formation of short 2–5 bp deletions (Kim et al., 2011; Sloan et al., 2017; Williams et al., 2013). Therefore, we explored whether the accelerated replication led to increased ribonucleotide incorporation, which may result in TOP1-dependent short deletions. To do so, we analyzed genomic ribonucleotide incorporation using alkaline gel migration assay. The results show no significant increase in ribonucleotide incorporation in RAS-expressing cells (Figures S7G and S7H), indicating that the RAS-induced accelerated replication and DNA damage are not the result of increased incorporation of ribonucleotides.

Our results show that TOP1-induced accelerated replication generates DNA damage. It has previously been suggested that accelerated replication may impair DNA polymerase fidelity (Maya-Mendoza et al., 2018). Therefore, we explored the potential link between high TOP1 expression and accumulation of mutations in cancer. For this, we analyzed data from the Pan-Cancer Analysis of Whole Genomes (PCAWG) (Alexandrov et al., 2020). We defined high TOP1 expression as >2 SDs of the mean TOP1 expression in healthy tissue samples; normal TOP1 expression as values within the range of ±2 SDs of the mean expression in healthy samples (Figure 7A). Next, we compared the number of insertions or deletions (indels) per patient tumor sample between the two groups; the results showed a significant increase in the mean indel count per patient in high, compared with normal, TOP1 (Figure 7B). In addition, analysis of the indel spectra revealed an increase in a single thymine insertion or deletion in long (>5 bp) thymine mononucleotide repeats in the high, compared with normal, TOP-expressing tumors (Figures 7D–7F). These 1 bp indels correspond to indel signatures ID1 and ID2, as characterized by COSMIC (Tate et al., 2019), which are suggested to result from slippage during DNA replication (Alexandrov et al., 2020). Interestingly, the ID4 signature, which was recently shown to result from TOP1 cleavage at incorporated ribonucleotides mainly in RNaseH2-deficient cells and tumors (Reijns et al., 2022), was not associated with the TOP1 expression level (Figures 7D–7F). In this regard, it is worth noting that only 2/1,012 analyzed samples were RNaseH2 null, of which one tumor showed the expected ID4 signature (Figures S8A and S8B).

Impaired DNA polymerase fidelity due to accelerated rate may also lead to an increase in single base substitutions (SBSs). Indeed, a significant increase in the mean SBS count per patient was found in high, compared with normal, TOP1-expressing tumor samples (Figure 7C). In addition, SBS spectra analysis showed an increase in SBS9 signature in high TOP1 tumors (Figures 7G–7I). Interestingly, SBS9 is proposed to result from hypermutation induced by the translesion DNA polymerase η (Tate et al., 2019). Thus, overall, these results indicate that increased TOP1 is associated with DNA replication mutagenesis.

DISCUSSION

In this study, we highlight the importance of TOP1 equilibrium in the regulation of R-loop homeostasis to ensure faithful DNA replication and genome integrity (Figure S8C). We show that an increase in TOP1 expression leads to a reduction in R-loop levels promoting replication fork acceleration resulting in DNA damage.

TOP1 downregulation or inhibition increases R-loops and slows the replication rate (Promonet et al., 2020; Tuduri et al., 2009; Xu and Her, 2015). Moreover, TOP1 knockout mice are embryonically lethal (Morham et al., 1996). In contrast to TOP1 deficiency, little is known about the effect of excess TOP1.

(D–F) DNA combing analysis of Ctrl and RNaseH1 HEK-293 cells, as indicated in (A). Fork rate (kb/min); at least 250 fibers per condition were analyzed (D). Fork distance (kb); at least 130 fibers per condition were analyzed (E). Sister fork symmetry; at least 90 fibers per condition were analyzed (F). Means are indicated, and red lines indicate medians. Data are the summary of two independent experiments. Dashed green line indicates asymmetry ratio threshold (F).
(G and H) 53BP1 (green) foci in HEK-293 cells, as indicated in (A). Representative images (G). Percentage of cells with indicated number of foci per nucleus in Ctrl (n = 1,120) and RNaseH1 (n = 1,111) (H). Data are the summary of two independent experiments.
(D–H) p values were calculated by Mann-Whitney rank-sum test. ns, non-significant; ****$p < 0.0001$. Scale bars, 10 μm.

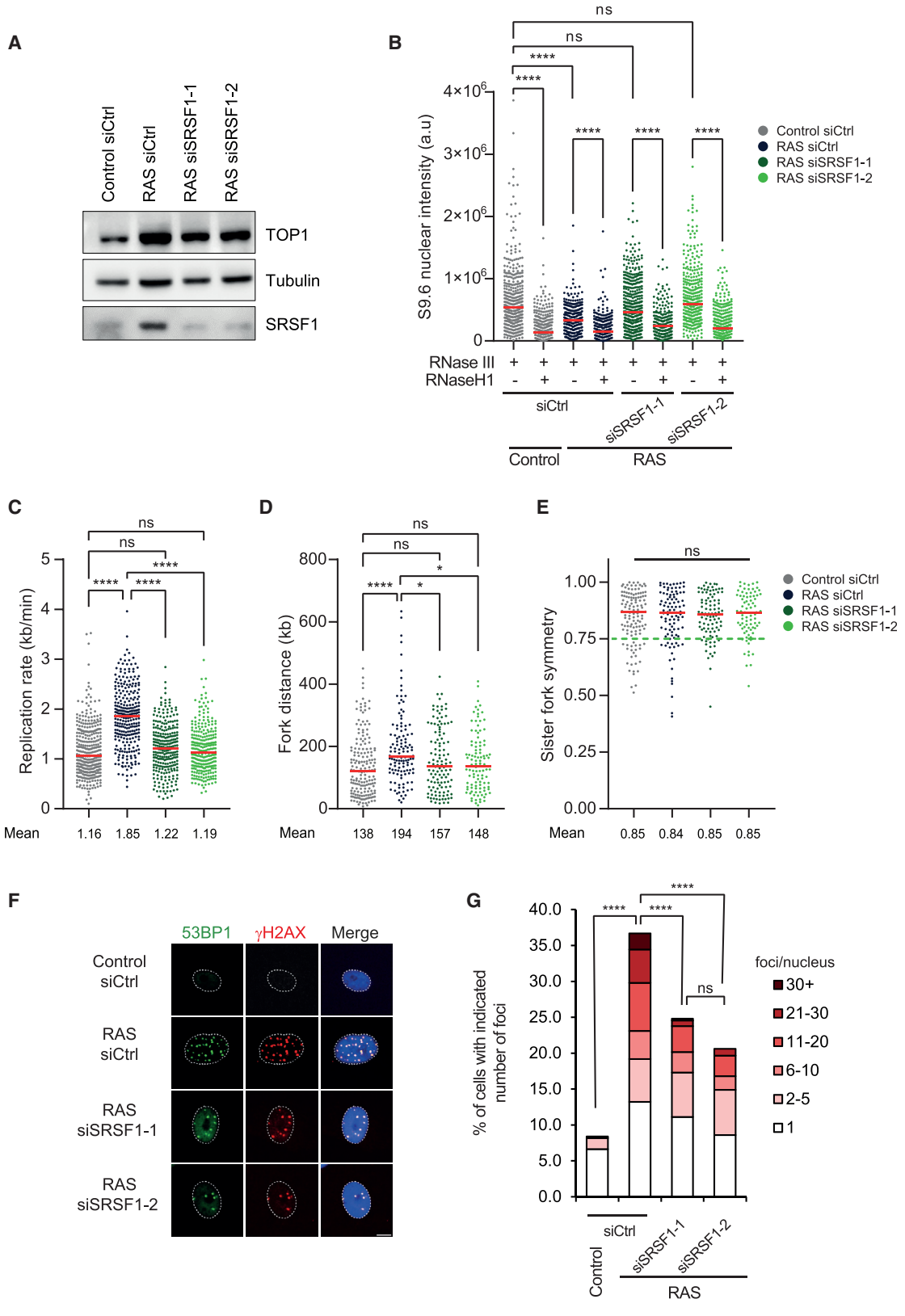

(legend on next page)

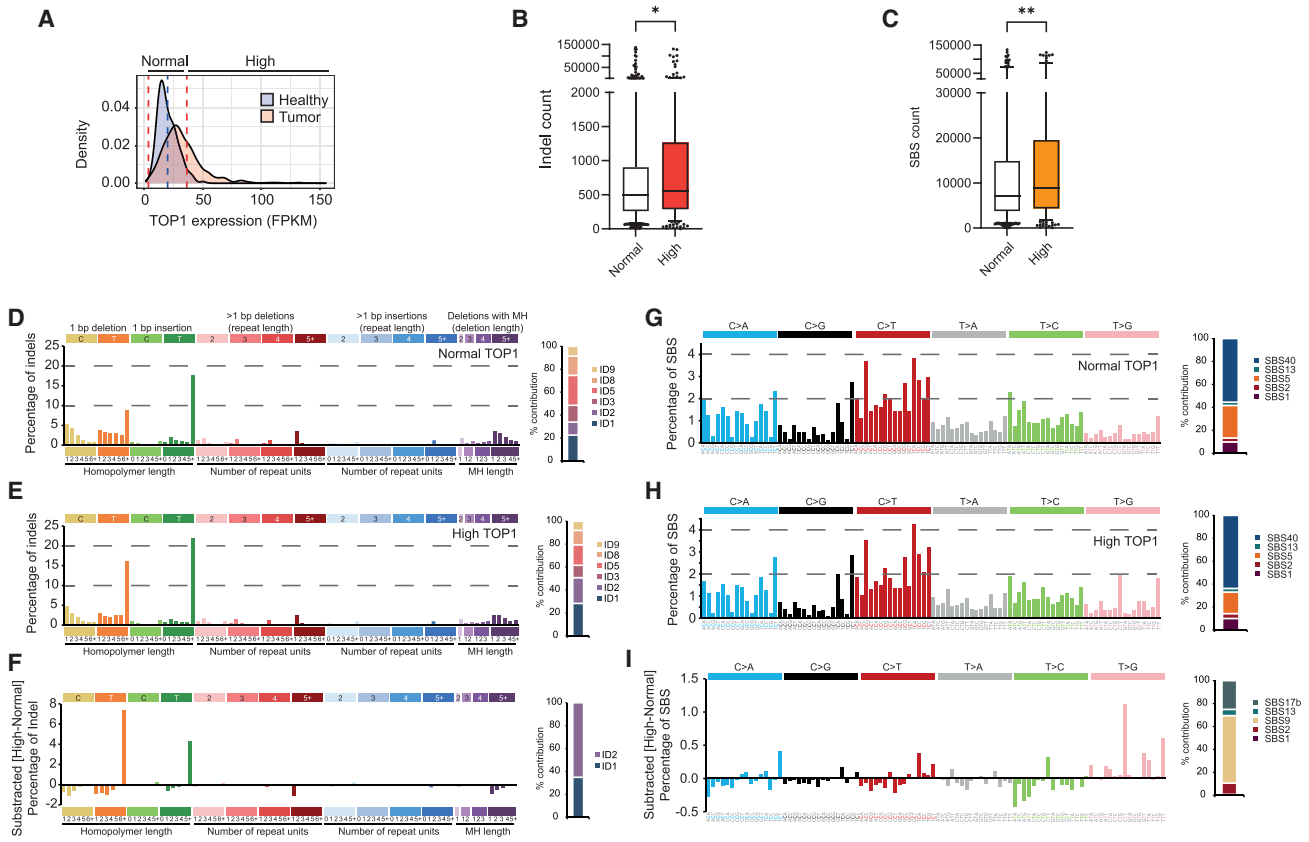

Figure 7. High TOP1 is associated with increased replication related mutagenesis

(A) Histogram of TOP1 expression in healthy (blue) and tumor (red) samples. Dashed blue line indicates the mean TOP1 expression in healthy; dashed red lines indicate the ± 2 SDs of the mean TOP1 expression in healthy.

(B) Indel count is increased in high TOP1-expressing tumors. The box limits show from 25% to 75%, the center line shows the median, the whiskers show from 5% to 95%, and the data points show values outside the range.

(C) Single base substitution (SBS) count is increased in high TOP1-expressing tumors. Boxplot as described in (B).

(D–F) Indel mutational spectrum in normal TOP1-expression tumors (D), high TOP1-expression tumors (E), and subtracted high normal (F).

(G–I) SBS mutational spectrum in normal TOP1-expression tumors (G), high TOP1-expression tumors (H), and subtracted high normal (I). Student's t test. *p < 0.05; **p < 0.001.

TOP1 OE was associated with mutagenesis in yeast (Sloan et al., 2017) and increased DNA damage (Humbert et al., 2009), and elevated levels of TOP1 are found in several cancers (Figure S5B) (Grunnet et al., 2015; Lee et al., 2015; Nagy et al., 2017; Rømer et al., 2012). However, whether surplus TOP1 affects replication dynamics was unexplored. Here, we show that increased TOP1 expression reduces R-loops, accelerates DNA replication, and generates DNA damage (Figures 3 and 4). TOP1-dependent reduction of R-loops underlies replication fork acceleration, as RNaseH1 OE increased the rate of replication (Figure 5) and downregulation of SRSF1 in RAS cells restored both R-loop levels and replication rate (Figure 6). These results indicate that the accelerated replication resulted from TOP1-dependent R-loop dysregulation rather than TOP1 resolution of excess of supercoiling. Altogether, our results highlight the importance of a regulated expression of TOP1 for R-loop equilibrium, ensuring

Figure 6. R-loop level restoration rescues aberrant accelerated replication

(A) Protein levels of TOP1, Tubulin, and SRSF1 in ER:RAS-infected FSE cells with (RAS) or without (Ctrl) 4-OHT treatment and treated with two independent siRNAs against SRSF1 (siSRSF1-1 and siSRSF1-2) or non-targeting siRNA (siCtrl), as indicated.

(B) Mean nuclear fluorescence intensity of RNA-DNA hybrid antibody (S9.6) after nucleolar signal removal in Ctrl and RAS cells treated with siRNA, RNaseIII, and RNaseH1, as indicated. Red lines indicate medians.

(C–E) DNA combing analysis of Ctrl and RAS cells, as indicated in (A). Fork rate (kb/min); at least 270 fibers per condition were analyzed (D). Fork distance (kb); at least 100 fibers per condition were analyzed (E). Sister fork symmetry; at least 80 fibers per condition were analyzed (E). Means are indicated, and red lines indicate medians. Data are the summary of two independent experiment. Dashed green line indicates asymmetry ratio threshold (E).

(F and G) Immunostaining with γH2AX (red) and 53BP1 (green) in Ctrl and RAS cells as indicated, in (A). Representative images (F). Percentage of cells with indicated number of co-localized foci per nucleus; at least 380 nuclei per condition were analyzed (G). Data are the summary of two independent experiments. p values were calculated by Kruskal-Wallis test. ns, non-significant; *p < 0.05, ****p < 0.0001. Scale bar, 10 μm.

faithful DNA replication and genome integrity, as both excess and insufficient levels perturb DNA replication and lead to DNA damage.

Replication stress is mainly characterized by fork slowing and stalling generating DNA damage (Zeman and Cimprich, 2014). While this is largely accepted today, other forms of perturbed replication were reported in recent years. Among the emerging non-canonical forms of replication stress is replication fork acceleration. Previous studies found accelerated replication following downregulation of mRNA biogenesis genes, including *THOC1*, *PCID2*, and *GANP* (Bhatia et al., 2014; Domínguez-Sánchez et al., 2011), chromatin modifier interacting with RNA-binding factors (Salas-Armenteros et al., 2017), and origin licensing and firing genes *ORC1*, *CDC7*, *CDC6*, and *MCM4* (Sedlackova et al., 2020; Zhong et al., 2013). Importantly, no change in the expression levels of these genes was found in our RAS-expressing cells (Table S1; Figure 3A), supporting that deregulation of various processes underlie accelerated DNA replication.

Recently, accelerated replication was reported following dysregulation of cancer-associated genes, including OE of the oncogene *Spi-1* (Rimmele et al., 2010) and interferon-stimulated gene 15 (*ISG15*) (Raso et al., 2020), and following exposure to the developmental mitogen sonic hedgehog (Shh) (Tamayo-Orrego et al., 2020). Moreover, inhibition of PARP, a common antitumor agent that facilitates repair of DNA damage, accelerated DNA replication and promoted genomic instability (Maya-Mendoza et al., 2018; Sugimura et al., 2008). Interestingly, PARP inhibition delocalizes TOP1 from the nucleolus to the nucleoplasm (Das et al., 2016), where replication of the bulk of the genome takes place. In light of our results, the higher levels of TOP1 in the nucleoplasm after PARP inhibition may contribute to the observed accelerated replication.

Most studies reporting accelerated DNA replication also observed an increase in DNA damage. However, whether the accelerated replication directly causes damage remained unknown. We addressed this question and found reduced DNA damage following normalized accelerated replication (Figures 2 and S3), indicating that the increased replication rate indeed drives DNA damage formation. We further investigated the possibility that DNA damage induced in RAS cells may also result directly from TOP1 elevated levels by TDP1 OE. As TDP1 OE had no effect on the damage levels in TOP1-overexpressing cells (Figures S7D and S7E), it can be concluded that the DNA damage is not a result of excess DNA-bound TOP1ccs. Furthermore, RNaseH1 OE accelerated DNA replication and increased DNA damage in a TOP1-independent manner (Figure 5). These results are in agreement with the results from the HU/APH experiments, in which replication restoration led to a decrease in DNA damage while the level of TOP1 remained high (Figure S6K). Altogether, our results indicate that TOP1-induced damage is not the cause for the accumulated DNA damage in cells with accelerated replication.

Previous studies of oncogene-induced replication stress showed that slow replication-induced DNA damage resulted from insufficient levels of dNTPs (Bester et al., 2011; Primo and Teixeira, 2020). However, in our study, supplementation of dNTPs did not affect damage levels in RAS-expressing cells, suggesting that the damage is not the result of a dNTP deficiency, as expected by the observed accelerated replication, which would have been hindered and stalled if dNTPs were limited. Previous studies showed that an increase in R-loops may lead to stalling of replication forks, resulting in fork asymmetry and DNA damage (García-Muse and Aguilera, 2019). Interestingly, this was found even when replication was accelerated due to chromatin changes (Salas-Armenteros et al., 2017). However, in our study, R-loops were reduced without fork asymmetry, suggesting that the damage is not caused by R-loop accumulation. Altogether, our results support the notion that accelerated replication-induced DNA damage is mechanistically different from that induced by fork stalling.

It was suggested that accelerated replication may impair DNA polymerase fidelity, leading to DNA damage by increased mutagenesis (Kunkel, 2004; Maya-Mendoza et al., 2018). Our PCAWG data analysis indeed revealed in tumors with high TOP1 expression an increase in mutagenesis, especially in replication slippage (ID1, ID2) and DNA pol η hypermutation (SBS9) signatures. In light of our results, TOP1-induced accelerated replication may promote mutagenesis, associated with DNA replication. Interestingly, RAS-expressing cells show an increase in single-stranded DNA (ssDNA; phosphorylated Chk1) and markers of under-replicated regions (fragile sites) (Figures 1I, 1J, S2E, and S2F), raising the possibility that excess TOP1 and accelerated replication may perturb DNA replication and its proofreading and thus leave behind ssDNA lesions that may be converted to DSBs (Palmerola et al., 2022). Further studies are required to shed light on the molecular mechanism(s) underlying accelerated replication-induced DNA damage.

Mutated RAS OE results in various effects on replication dynamics. Maya-Mendoza et al. (2015) reported a small, yet significant, increase in replication rate at the hyperproliferative phase, prior to senescence onset. However, this was followed by a decrease in replication rate and an increase in DNA damage levels (Maya-Mendoza et al., 2015). In another study, Di Micco et al. (2006) showed that RAS OE in CHK2-deficient cells prevented senescence and increased origin firing. Kotsantis et al. (2016) reported that RAS OE resulted in slow replication and DNA damage. The authors further showed that RAS upregulated the general transcription factor TATA-box binding protein (TBP) at the hyperproliferative phase, which led to an increase in RNA synthesis, accumulation of R-loops, and slow rate and DNA damage (Kotsantis et al., 2016). In our study, however, RAS OE did not change TBP expression (Table S1). Furthermore, RAS expression in our study reduced R-loops due to TOP1 OE. Interestingly, as previously shown, RAS upregulates MYC (Figure S5E) (Kerkhoff et al., 1998), which can in turn contribute to TOP1 upregulation and even recruit it to transcribed genes and stimulate its activity (Das et al., 2022). It is worth noting that in different cellular systems, MYC OE had different effects on DNA replication dynamics (Ben-David et al., 2014; Guerrero Llobet et al., 2022). Altogether, we suggest that RAS-induced MYC expression may promote TOP1 OE and, furthermore, that MYC may stimulate TOP1 activity. Thus, overall, different factors may underlie the various effects of RAS OE on the replication dynamics. One possible factor is a different RAS OE level, since a dose-dependent effect of RAS expression on cell proliferation and senescence was previously shown (Sarkisian et al., 2007), which may reflect differences in replication dynamics and DNA damage.

Another possible factor is the use of different cellular systems with different genetic backgrounds. It is well established that there is accumulation of genetic changes during cell culturing of cancer cell lines, leading to variations in gene-expression patterns that may differently affect the replication dynamics and DNA damage (Ben-David et al., 2018; Kim et al., 2017; Weissbein et al., 2014). Altogether, the plasticity of RAS-induced replication stress found in different studies suggests that the genetic background of oncogenic cells may affect the phenotype and hence should be reflected in the treatment for patients with cancer.

Altogether, our results indicate that TOP1 is a crucial factor for genome integrity, by tightly regulating replication dynamics. This further highlights the importance of TOP1-dependent R-loop homeostasis in replication regulation, as unbalanced levels alter replication dynamics and promote genomic instability (Figure S8C). These results are highly important for understanding early events leading to cancer development, as different mechanisms may underlie the oncogene-induced replication perturbation driving genomic instability. They reveal the complex nature of oncogene-induced replication stress, which should be taken into consideration when replication inhibitors are considered as a therapeutic tool for cancer (Keller et al., 2022).

STAR★METHODS

Detailed methods are provided in the online version of this paper and include the following:

- KEY RESOURCES TABLE
- RESOURCE AVAILABILITY
  - Lead contact
  - Materials availability
  - Data and code availability
- EXPERIMENTAL MODEL AND SUBJECT DETAILS
  - Cell Culture
  - Plasmids
- METHOD DETAILS
  - Replication dynamics using DNA combing
  - Immunofluorescence staining
  - Metaphase chromosome preparation and fragile site analysis
  - Western blot analysis
  - Population doublings
  - RNA sequencing analysis
  - Gene correlation analysis in GEPIA
  - RNA analysis
  - siRNA
  - Cell cycle analysis
  - DRIP-qPCR
  - Alkaline gel electrophoresis
  - Mutation analysis
  - Viability assay
- QUANTIFICATION AND STATISTICAL ANALYSIS

SUPPLEMENTAL INFORMATION

Supplemental information can be found online at https://doi.org/10.1016/j.celrep.2022.111397.

ACKNOWLEDGMENTS

This research was supported by grants from the Israel Science Foundation (grant nos. 176/11 and 1284/18), the Israeli Centers of Research Excellence (I-CORE), and Gene Regulation in Complex Human Disease, Center No. 41/11, and by the ISF-NSFC joint program (grant no. 2535/16) to B.K. and by grants from the Agencia Estatal de Investigación from the Spanish Ministry of Science and Innovation (PID2019-104270GB-I00/BMC), the European Research Council (ERC2014 AdG669898 TARLOOP), the European Union (FEDER), and the Foundation "Vencer el Cancer" to A.A. The authors thank Dr. Naomi Melamed-Book for her assistance in confocal microscopy and the Mantoux Bioinformatics Institute of the Nancy and Stephen Grand Israel National Center for Personalized Medicine, Weizmann Institute of Science, for assistance in deep sequencing and bioinformatics analysis. The authors thank the members of the Kerem lab for thoughtful discussions and advice.

AUTHOR CONTRIBUTIONS

Conceptualization, D.S. and B.K.; methodology, D.S., A.A., and B.K.; investigation, D.S., S.B., A.S., M.I.-T.S., Y.S.O., A.A., and B.K.; visualization, D.S. and B.K.; writing – original draft, D.S. and B.K.; writing – review & editing, D.S., M.I.-T.S., A.A., and B.K.; funding acquisition, A.A. and B.K.

DECLARATION OF INTERESTS

The authors declare no competing interests.

Received: March 5, 2022
Revised: June 26, 2022
Accepted: August 31, 2022
Published: September 27, 2022

REFERENCES

Abulaiti, A., Fikaris, A.J., Tsygankova, O.M., and Meinkoth, J.L. (2006). Ras induces chromosome instability and abrogation of the DNA damage response. Cancer Res. *66*, 10505–10512. https://doi.org/10.1158/0008-5472.CAN-06-2351.

Aird, K.M., Zhang, G., Li, H., Tu, Z., Bitler, B.G., Garipov, A., Wu, H., Wei, Z., Wagner, S.N., Herlyn, M., et al. (2013). Suppression of nucleotide metabolism underlies the establishment and maintenance of oncogene-induced senescence. Cell Rep. *3*, 1252–1265. https://doi.org/10.1016/j.celrep.2013.03.004.

Alexandrov, L.B., Kim, J., Haradhvala, N.J., Huang, M.N., Tian Ng, A.W., Wu, Y., Boot, A., Covington, K.R., Gordenin, D.A., Bergstrom, E.N., et al. (2020). The repertoire of mutational signatures in human cancer. Nature *578*, 94–101. https://doi.org/10.1038/s41586-020-1943-3.

Anders, S., Pyl, P.T., and Huber, W. (2015). HTSeq–a Python framework to work with high-throughput sequencing data. Bioinformatics *31*, 166–169. https://doi.org/10.1093/bioinformatics/btu638.

Bartkova, J., Rezaei, N., Liontos, M., Karakaidos, P., Kletsas, D., Issaeva, N., Vassiliou, L.-V.F., Kolettas, E., Niforou, K., Zoumpourlis, V.C., et al. (2006). Oncogene-induced senescence is part of the tumorigenesis barrier imposed by DNA damage checkpoints. Nature *444*, 633–637. https://doi.org/10.1038/nature05268.

Ben-David, E., Bester, A.C., Shifman, S., and Kerem, B. (2014). Transcriptional dynamics in colorectal carcinogenesis: new insights into the role of c-myc and miR17 in benign to cancer transformation. Cancer Res. *74*, 5532–5540. https://doi.org/10.1158/0008-5472.CAN-14-0932.

Ben-David, U., Siranosian, B., Ha, G., Tang, H., Oren, Y., Hinohara, K., Strathdee, C.A., Dempster, J., Lyons, N.J., Burns, R., et al. (2018). Genetic and transcriptional evolution alters cancer cell line drug response. Nature *560*, 325–330. https://doi.org/10.1038/s41586-018-0409-3.

Bensimon, A., Simon, A., Chiffaudel, A., Croquette, V., Heslot, F., and Bensimon, D. (1994). Alignment and sensitive detection of DNA by a moving interface. Science *265*, 2096–2098.

Bester, A.C., Roniger, M., Oren, Y.S., Im, M.M., Sarni, D., Chaoat, M., Bensimon, A., Zamir, G., Shewach, D.S., and Kerem, B. (2011). Nucleotide deficiency promotes genomic instability in early stages of cancer development. Cell *145*, 435–446. https://doi.org/10.1016/j.cell.2011.03.044.

Bhatia, V., Barroso, S.I., García-Rubio, M.L., Tumini, E., Herrera-Moyano, E., and Aguilera, A. (2014). BRCA2 prevents R-loop accumulation and associates with TREX-2 mRNA export factor PCID2. Nature *511*, 362–365. https://doi.org/10.1038/nature13374.

Cheng, C.H., and Kuchta, R.D. (1993). DNA polymerase epsilon: aphidicolin inhibition and the relationship between polymerase and exonuclease activity. Biochemistry *32*, 8568–8574.

Conti, C., Saccà, B., Herrick, J., Lalou, C., Pommier, Y., and Bensimon, A. (2007). Replication fork velocities at adjacent replication origins are coordinately modified during DNA replication in human cells. Mol. Biol. Cell *18*, 3059–3067. https://doi.org/10.1091/mbc.e06-08-0689.

Courbet, S., Gay, S., Arnoult, N., Wronka, G., Anglana, M., Brison, O., and Debatisse, M. (2008). Replication fork movement sets chromatin loop size and origin choice in mammalian cells. Nature *455*, 557–560. https://doi.org/10.1038/nature07233.

Das, S.K., Rehman, I., Ghosh, A., Sengupta, S., Majumdar, P., Jana, B., and Das, B.B. (2016). Poly(ADP-ribose) polymers regulate DNA topoisomerase I (Top1) nuclear dynamics and camptothecin sensitivity in living cells. Nucleic Acids Res. *44*, 8363–8375. https://doi.org/10.1093/nar/gkw665.

Das, S.K., Kuzin, V., Cameron, D.P., Sanford, S., Jha, R.K., Nie, Z., Rosello, M.T., Holewinski, R., Andresson, T., Wisniewski, J., et al. (2022). MYC assembles and stimulates topoisomerases 1 and 2 in a "topoisome. Mol. Cell *82*, 140–158, e12. https://doi.org/10.1016/j.molcel.2021.11.016.

Denko, N.C., Giaccia, A.J., Stringer, J.R., and Stambrook, P.J. (1994). The human Ha-ras oncogene induces genomic instability in murine fibroblasts within one cell cycle. Proc. Natl. Acad. Sci. USA *91*, 5124–5128.

Domínguez-Sánchez, M.S., Barroso, S., Gómez-González, B., Luna, R., and Aguilera, A. (2011). Genome instability and transcription elongation impairment in human cells depleted of THO/TREX. PLoS Genet. *7*, e1002386. https://doi.org/10.1371/journal.pgen.1002386.

Dominguez-Sola, D., Ying, C.Y., Grandori, C., Ruggiero, L., Chen, B., Li, M., Galloway, D.A., Gu, W., Gautier, J., and Dalla-Favera, R. (2007). Non-transcriptional control of DNA replication by c-Myc. Nature *448*, 445–451. https://doi.org/10.1038/nature05953.

Downward, J. (2003). Targeting RAS signalling pathways in cancer therapy. Nat. Rev. Cancer *3*, 11–22. https://doi.org/10.1038/nrc969.

Ewald, B., Sampath, D., and Plunkett, W. (2007). H2AX phosphorylation marks gemcitabine-induced stalled replication forks and their collapse upon S-phase checkpoint abrogation. Mol. Cancer Ther. *6*, 1239–1248. https://doi.org/10.1158/1535-7163.MCT-06-0633.

Flach, J., Bakker, S.T., Mohrin, M., Conroy, P.C., Pietras, E.M., Reynaud, D., Alvarez, S., Diolaiti, M.E., Ugarte, F., Forsberg, E.C., et al. (2014). Replication stress is a potent driver of functional decline in ageing haematopoietic stem cells. Nature *512*, 198–202. https://doi.org/10.1038/nature13619.

Fragkos, M., Ganier, O., Coulombe, P., and Méchali, M. (2015). DNA replication origin activation in space and time. Nat. Rev. Mol. Cell Biol. *16*, 360–374. https://doi.org/10.1038/nrm4002.

Gaillard, H., García-Muse, T., and Aguilera, A. (2015). Replication stress and cancer. Nat. Rev. Cancer *15*, 276–289. https://doi.org/10.1038/nrc3916.

Galanos, P., Vougas, K., Walter, D., Polyzos, A., Maya-Mendoza, A., Haagensen, E.J., Kokkalis, A., Roumelioti, F.-M., Gagos, S., Tzetis, M., et al. (2016). Chronic p53-independent p21 expression causes genomic instability by deregulating replication licensing. Nat. Cell Biol. *18*, 777–789. https://doi.org/10.1038/ncb3378.

García-Muse, T., and Aguilera, A. (2019). R loops: from physiological to pathological roles. Cell *179*, 604–618. https://doi.org/10.1016/j.cell.2019.08.055.

García-Rubio, M., Barroso, S.I., and Aguilera, A. (2018). In Genome Instability. Methods in Molecular Biology, *1672*, M. Muzi-Falconi and G. Brown, eds. (New York, NY: Humana Press). https://doi.org/10.1007/978-1-4939-7306-4_24.

Ge, X.Q., and Blow, J.J. (2010). Chk1 inhibits replication factory activation but allows dormant origin firing in existing factories. J. Cell Biol. *191*, 1285–1297. https://doi.org/10.1083/jcb.201007074.

Ge, X.Q., Jackson, D.A., and Blow, J.J. (2007). Dormant origins licensed by excess Mcm2 7 are required for human cells to survive replicative stress. Genes Dev. *21*, 3331–3341. https://doi.org/10.1101/gad.457807.

Glover, T.W., Berger, C., Coyle, J., and Echo, B. (1984). DNA polymerase alpha inhibition by aphidicolin induces gaps and breaks at common fragile sites in human chromosomes. Hum. Genet. *67*, 136–142.

Greenwood, S.K., Hill, R.B., Sun, J.T., Armstrong, M.J., Johnson, T.E., Gara, J.P., and Galloway, S.M. (2004). Population doubling: a simple and more accurate estimation of cell growth suppression in the in vitro assay for chromosomal aberrations that reduces irrelevant positive results. Environ. Mol. Mutagen. *43*, 36–44. https://doi.org/10.1002/em.10207.

Grunnet, M., Calatayud, D., Schultz, N.A., Hasselby, J.P., Mau-Sørensen, M., Brünner, N., and Stenvang, J. (2015). TOP1 gene copy numbers are increased in cancers of the bile duct and pancreas. Scand. J. Gastroenterol. *50*, 485–494. https://doi.org/10.3109/00365521.2014.980318.

Guerrero Llobet, S., Bhattacharya, A., Everts, M., Kok, K., van der Vegt, B., Fehrmann, R.S.N., and van Vugt, M.A.T.M. (2022). An mRNA expression-based signature for oncogene-induced replication-stress. Oncogene *41*, 1216–1224. https://doi.org/10.1038/s41388-021-02162-0.

Halazonetis, T.D., Gorgoulis, V.G., and Bartek, J. (2008). An oncogene-induced DNA damage model for cancer development. Science *319*, 1352–1355. https://doi.org/10.1126/science.1140735.

Hanahan, D., and Weinberg, R.A. (2011). Hallmarks of cancer: the next generation. Cell *144*, 646–674. https://doi.org/10.1016/j.cell.2011.02.013.

Herrick, J., and Bensimon, A. (1999). Single molecule analysis of DNA replication. Biochimie *81*, 859–871.

Hübschmann, D., Jopp-Saile, L., Andresen, C., Krämer, S., Gu, Z., Heilig, C.E., Kreutzfeldt, S., Teleanu, V., Fröhling, S., Eils, R., et al. (2021). Analysis of mutational signatures with yet another package for signature analysis. Genes, Chromosom. Cancer *60*, 314–331. https://doi.org/10.1002/gcc.22918.

Humbert, N., Martien, S., Augert, A., Da Costa, M., Mauen, S., Abbadie, C., de Launoit, Y., Gil, J., and Bernard, D. (2009). A genetic screen identifies topoisomerase 1 as a regulator of senescence. Cancer Res. *69*, 4101–4106. https://doi.org/10.1158/0008-5472.CAN-08-2864.

Ikegami, S., Taguchi, T., Ohashi, M., Oguro, M., Nagano, H., and Mano, Y. (1978). Aphidicolin prevents mitotic cell division by interfering with the activity of DNA polymerase-alpha. Nature *275*, 458–460.

Keller, K.M., Krausert, S., Gopisetty, A., Luedtke, D., Koster, J., Schubert, N.A., Rodríguez, A., van Hooff, S.R., Stichel, D., Dolman, M.E.M., et al. (2022). Target Actionability Review: a systematic evaluation of replication stress as a therapeutic target for paediatric solid malignancies. Eur. J. Cancer *162*, 107–117. https://doi.org/10.1016/j.ejca.2021.11.030.

Kerkhoff, E., Houben, R., Löffler, S., Troppmair, J., Lee, J.-E., and Rapp, U.R. (1998). Regulation of c-myc expression by Ras/Raf signalling. Oncogene *16*, 211–216. https://doi.org/10.1038/sj.onc.1201520.

Kim, D., Pertea, G., Trapnell, C., Pimentel, H., Kelley, R., and Salzberg, S.L. (2013). TopHat2: accurate alignment of transcriptomes in the presence of insertions, deletions and gene fusions. Genome Biol. *14*, R36. https://doi.org/10.1186/gb-2013-14-4-r36.

Kim, M., Rhee, J.-K., Choi, H., Kwon, A., Kim, J., Lee, G.D., Jekarl, D.W., Lee, S., Kim, Y., and Kim, T.-M. (2017). Passage-dependent accumulation of somatic mutations in mesenchymal stromal cells during in vitro culture revealed by whole genome sequencing. Sci. Rep. *7*, 14508. https://doi.org/10.1038/s41598-017-15155-5.

Kim, N., Huang, S.N., Williams, J.S., Li, Y.C., Clark, A.B., Cho, J.-E., Kunkel, T.A., Pommier, Y., and Jinks-Robertson, S. (2011). Mutagenic processing of ribonucleotides in DNA by yeast topoisomerase I. Science *332*, 1561–1564. https://doi.org/10.1126/science.1205016.

Kotsantis, P., Silva, L.M., Irmscher, S., Jones, R.M., Folkes, L., Gromak, N., and Petermann, E. (2016). Increased global transcription activity as a

mechanism of replication stress in cancer. Nat. Commun. *7*, 13087. https://doi.org/10.1038/ncomms13087.

Koundrioukoff, S., Carignon, S., Técher, H., Letessier, A., Brison, O., and Debatisse, M. (2013). Stepwise activation of the ATR signaling pathway upon increasing replication stress impacts fragile site integrity. PLoS Genet. *9*, e1003643. https://doi.org/10.1371/journal.pgen.1003643.

Kunkel, T.A. (2004). DNA replication fidelity. J. Biol. Chem. *279*, 16895–16898. https://doi.org/10.1074/jbc.R400006200.

Lee, Y.-C., Lee, C.-H., Tsai, H.-P., An, H.-W., Lee, C.-M., Wu, J.-C., Chen, C.-S., Huang, S.-H., Hwang, J., Cheng, K.-T., et al. (2015). Targeting of topoisomerase I for prognoses and therapeutics of camptothecin-resistant ovarian cancer. PLoS One *10*, e0132579. https://doi.org/10.1371/journal.pone.0132579.

Li, X., and Manley, J.L. (2005). Inactivation of the SR protein splicing factor ASF/SF2 results in genomic instability. Cell *122*, 365–378. https://doi.org/10.1016/j.cell.2005.06.008.

Love, M.I., Huber, W., and Anders, S. (2014). Moderated estimation of fold change and dispersion for RNA-seq data with DESeq2. Genome Biol. *15*, 550. https://doi.org/10.1186/s13059-014-0550-8.

Lukas, C., Savic, V., Bekker-Jensen, S., Doil, C., Neumann, B., Sølvhøj Pedersen, R., Grøfte, M., Chan, K.L., Hickson, I.D., Bartek, J., et al. (2011). 53BP1 nuclear bodies form around DNA lesions generated by mitotic transmission of chromosomes under replication stress. Nat. Cell Biol. *13*, 243–253. https://doi.org/10.1038/ncb2201.

Macheret, M., and Halazonetis, T.D. (2015). DNA replication stress as a hallmark of cancer. Annu. Rev. Pathol. Mech. Dis. *10*, 425–448. https://doi.org/10.1146/annurev-pathol-012414-040424.

Maya-Mendoza, A., Ostrakova, J., Kosar, M., Hall, A., Duskova, P., Mistrik, M., Merchut-Maya, J.M., Hodny, Z., Bartkova, J., Christensen, C., et al. (2015). Myc and Ras oncogenes engage different energy metabolism programs and evoke distinct patterns of oxidative and DNA replication stress. Mol. Oncol. *9*, 601–616. https://doi.org/10.1016/j.molonc.2014.11.001.

Maya-Mendoza, A., Moudry, P., Merchut-Maya, J.M., Lee, M., Strauss, R., and Bartek, J. (2018). High speed of fork progression induces DNA replication stress and genomic instability. Nature *559*, 279–284. https://doi.org/10.1038/s41586-018-0261-5.

Di Micco, R., Fumagalli, M., Cicalese, A., Piccinin, S., Gasparini, P., Luise, C., Schurra, C., Garre', M., Giovanni Nuciforo, P., Bensimon, A., et al. (2006). Oncogene-induced senescence is a DNA damage response triggered by DNA hyper-replication. Nature *444*, 638–642. https://doi.org/10.1038/nature05327.

Miron, K., Golan-Lev, T., Dvir, R., Ben-David, E., and Kerem, B. (2015). Oncogenes create a unique landscape of fragile sites. Nat. Commun. *6*, 7094. https://doi.org/10.1038/ncomms8094.

Morham, S.G., Kluckman, K.D., Voulomanos, N., and Smithies, O. (1996). Targeted disruption of the mouse topoisomerase I gene by camptothecin selection. Mol. Cell Biol. *16*, 6804–6809.

Nagy, Á., Pongor, L.S., Szabó, A., Santarpia, M., and Győrffy, B. (2017). KRAS driven expression signature has prognostic power superior to mutation status in non-small cell lung cancer. Int. J. Cancer *140*, 930–937. https://doi.org/10.1002/ijc.30509.

Negrini, S., Gorgoulis, V.G., and Halazonetis, T.D. (2010). Genomic instability — an evolving hallmark of cancer. Nat. Rev. Mol. Cell Biol. *11*, 220–228. https://doi.org/10.1038/nrm2858.

Palmerola, K.L., Amrane, S., De Los Angeles, A., Xu, S., Wang, N., de Pinho, J., Zuccaro, M.V., Taglialatela, A., Massey, D.J., Turocy, J., et al. (2022). Replication stress impairs chromosome segregation and preimplantation development in human embryos. Cell. https://doi.org/10.1016/j.cell.2022.06.028.

Pommier, Y. (2006). Topoisomerase I inhibitors: camptothecins and beyond. Nat. Rev. Cancer *6*, 789–802. https://doi.org/10.1038/nrc1977.

Pommier, Y., Barcelo, J.M., Rao, V.A., Sordet, O., Jobson, A.G., Thibaut, L., Miao, Z., Seiler, J.A., Zhang, H., Marchand, C., et al. (2006). Repair of Topoisomerase I-Mediated DNA Damage, pp. 179–229.

Pommier, Y., Sun, Y., Huang, S.N., and Nitiss, J.L. (2016). Roles of eukaryotic topoisomerases in transcription, replication and genomic stability. Nat. Rev. Mol. Cell Biol. *17*, 703–721. https://doi.org/10.1038/nrm.2016.111.

Primo, L.M.F., and Teixeira, L.K. (2020). DNA replication stress: oncogenes in the spotlight. Genet. Mol. Biol. *43*. https://doi.org/10.1590/1678-4685gmb-2019-0138.

Promonet, A., Padioleau, I., Liu, Y., Sanz, L., Biernacka, A., Schmitz, A.-L., Skrzypczak, M., Sarrazin, A., Mettling, C., Rowicka, M., et al. (2020). Topoisomerase 1 prevents replication stress at R-loop-enriched transcription termination sites. Nat. Commun. *11*, 3940. https://doi.org/10.1038/s41467-020-17858-2.

Pylayeva-Gupta, Y., Grabocka, E., and Bar-Sagi, D. (2011). RAS oncogenes: weaving a tumorigenic web. Nat. Rev. Cancer *11*, 761–774. https://doi.org/10.1038/nrc3106.

Raso, M.C., Djoric, N., Walser, F., Hess, S., Schmid, F.M., Burger, S., Knobeloch, K.-P., and Penengo, L. (2020). Interferon-stimulated gene 15 accelerates replication fork progression inducing chromosomal breakage. J. Cell Biol. *219*. https://doi.org/10.1083/jcb.202002175.

Reijns, M.A.M., Bubeck, D., Gibson, L.C.D., Graham, S.C., Baillie, G.S., Jones, E.Y., and Jackson, A.P. (2011). The structure of the human RNase H2 complex defines key interaction interfaces relevant to enzyme function and human Disease. J. Biol. Chem. *286*, 10530–10539. https://doi.org/10.1074/jbc.M110.177394.

Reijns, M.A.M., Rabe, B., Rigby, R.E., Mill, P., Astell, K.R., Lettice, L.A., Boyle, S., Leitch, A., Keighren, M., Kilanowski, F., et al. (2012). Enzymatic removal of ribonucleotides from DNA is essential for mammalian genome integrity and development. Cell *149*, 1008–1022. https://doi.org/10.1016/j.cell.2012.04.011.

Reijns, M.A.M., Parry, D.A., Williams, T.C., Nadeu, F., Hindshaw, R.L., Rios Szwed, D.O., Nicholson, M.D., Carroll, P., Boyle, S., Royo, R., et al. (2022). Signatures of TOP1 transcription-associated mutagenesis in cancer and germline. Nature *602*, 623–631. https://doi.org/10.1038/s41586-022-04403-y.

Rimmele, P., Komatsu, J., Hupe, P., Roulin, C., Barillot, E., Dutreix, M., Conseiller, E., Bensimon, A., Moreau-Gachelin, F., and Guillouf, C. (2010). Spi-1/PU.1 oncogene accelerates DNA replication fork elongation and promotes genetic instability in the absence of DNA breakage. Cancer Res. *70*, 6757–6766. https://doi.org/10.1158/0008-5472.CAN-09-4691.

Rømer, M.U., Jensen, N.F., Nielsen, S.L., Müller, S., Nielsen, K.V., Nielsen, H.J., and Brünner, N. (2012). TOP1 gene copy numbers in colorectal cancer samples and cell lines and their association to in vitro drug sensitivity. Scand. J. Gastroenterol. *47*, 68–79. https://doi.org/10.3109/00365521.2011.638393.

Saavedra, H.I., Knauf, J.A., Shirokawa, J.M., Wang, J., Ouyang, B., Elisei, R., Stambrook, P.J., and Fagin, J.A. (2000). The RAS oncogene induces genomic instability in thyroid PCCL3 cells via the MAPK pathway. Oncogene *19*, 3948–3954. https://doi.org/10.1038/sj.onc.1203723.

Salas-Armenteros, I., Pérez-Calero, C., Bayona-Feliu, A., Tumini, E., Luna, R., and Aguilera, A. (2017). Human <scp>THO</scp> –Sin3A interaction reveals new mechanisms to prevent R-loops that cause genome instability. EMBO J. *36*, 3532–3547. https://doi.org/10.15252/embj.201797208.

Santos-Pereira, J.M., and Aguilera, A. (2015). R loops: new modulators of genome dynamics and function. Nat. Rev. Genet. *16*, 583–597. https://doi.org/10.1038/nrg3961.

Sarkisian, C.J., Keister, B.A., Stairs, D.B., Boxer, R.B., Moody, S.E., and Chodosh, L.A. (2007). Dose-dependent oncogene-induced senescence in vivo and its evasion during mammary tumorigenesis. Nat. Cell Biol. *9*, 493–505. https://doi.org/10.1038/ncb1567.

Schindelin, J., Arganda-Carreras, I., Frise, E., Kaynig, V., Longair, M., Pietzsch, T., Preibisch, S., Rueden, C., Saalfeld, S., Schmid, B., et al. (2012). Fiji: an open-source platform for biological-image analysis. Nat. Methods *9*, 676–682. https://doi.org/10.1038/nmeth.2019.

Schneider, C.A., Rasband, W.S., and Eliceiri, K.W. (2012). NIH Image to ImageJ: 25 Years of Image Analysis. Nature Methods *9*, 671–675. https://doi.org/10.1038/nmeth.2089.

Schultz, L.B., Chehab, N.H., Malikzay, A., and Halazonetis, T.D. (2000). P53 binding protein 1 (53bp1) is an early participant in the cellular response to DNA double-strand breaks. J. Cell Biol. *151*, 1381–1390. https://doi.org/10.1083/jcb.151.7.1381.

Sears, R., Leone, G., DeGregori, J., and Nevins, J.R. (1999). Ras enhances myc protein stability. Mol. Cell *3*, 169–179. https://doi.org/10.1016/S1097-2765(00)80308-1.

Sedlackova, H., Rask, M.-B., Gupta, R., Choudhary, C., Somyajit, K., and Lukas, J. (2020). Equilibrium between nascent and parental MCM proteins protects replicating genomes. Nature *587*, 297–302. https://doi.org/10.1038/s41586-020-2842-3.

Skoog, L., and Nordenskjöld, B. (1971). Effects of hydroxyurea and 1-beta-D-arabinofuranosyl-cytosine on deoxyribonucleotide pools in mouse embryo cells. Eur. J. Biochem. *19*, 81–89.

Sloan, R., Huang, S.N., Pommier, Y., and Jinks-Robertson, S. (2017). Effects of camptothecin or TOP1 overexpression on genetic stability in Saccharomyces cerevisiae. DNA Repair *59*, 69–75. https://doi.org/10.1016/j.dnarep.2017.09.004.

Stephens, R.M., Yi, M., Kessing, B., Nissley, D.V., and McCormick, F. (2017). Tumor RAS gene expression levels are influenced by the mutational status of RAS genes and both upstream and downstream ras pathway genes. Cancer Inform. *16*, 117693511771194. https://doi.org/10.1177/1176935117711944.

Sugimura, K., Takebayashi, S., Taguchi, H., Takeda, S., and Okumura, K. (2008). PARP-1 ensures regulation of replication fork progression by homologous recombination on damaged DNA. J. Cell Biol. *183*, 1203–1212. https://doi.org/10.1083/jcb.200806068.

Tamayo-Orrego, L., Gallo, D., Racicot, F., Bemmo, A., Mohan, S., Ho, B., Salameh, S., Hoang, T., Jackson, A.P., Brown, G.W., et al. (2020). Sonic hedgehog accelerates DNA replication to cause replication stress promoting cancer initiation in medulloblastoma. Nat. Cancer *1*, 840–854. https://doi.org/10.1038/s43018-020-0094-7.

Tang, Z., Li, C., Kang, B., Gao, G., Li, C., and Zhang, Z. (2017). GEPIA: a web server for cancer and normal gene expression profiling and interactive analyses. Nucleic Acids Res. *45*, W98–W102. https://doi.org/10.1093/nar/gkx247.

Tate, J.G., Bamford, S., Jubb, H.C., Sondka, Z., Beare, D.M., Bindal, N., Boutselakis, H., Cole, C.G., Creatore, C., Dawson, E., et al. (2019). COSMIC: the catalogue of somatic mutations in cancer. Nucleic Acids Res. *47*, D941–D947. https://doi.org/10.1093/nar/gky1015.

Técher, H., Koundrioukoff, S., Carignon, S., Wilhelm, T., Millot, G.A., Lopez, B.S., Brison, O., and Debatisse, M. (2016). Signaling from Mus81-eme2-dependent DNA damage elicited by Chk1 deficiency modulates replication fork speed and origin usage. Cell Rep. *14*, 1114–1127. https://doi.org/10.1016/j.celrep.2015.12.093.

Tuduri, S., Crabbé, L., Conti, C., Tourrière, H., Holtgreve-Grez, H., Jauch, A., Pantesco, V., De Vos, J., Thomas, A., Theillet, C., et al. (2009). Topoisomerase I suppresses genomic instability by preventing interference between replication and transcription. Nat. Cell Biol. *11*, 1315–1324. https://doi.org/10.1038/ncb1984.

Wang, J., Duncan, D., Shi, Z., and Zhang, B. (2013). WEB-Based GEne SeT AnaLysis toolkit (WebGestalt): update 2013. Nucleic Acids Res. *41*, W77–W83. https://doi.org/10.1093/nar/gkt439.

Weissbein, U., Benvenisty, N., and Ben-David, U. (2014). Genome maintenance in pluripotent stem cells. J. Cell Biol. *204*, 153–163. https://doi.org/10.1083/jcb.201310135.

Williams, J.S., Smith, D.J., Marjavaara, L., Lujan, S.A., Chabes, A., and Kunkel, T.A. (2013). Topoisomerase 1-mediated removal of ribonucleotides from nascent leading-strand DNA. Mol. Cell *49*, 1010–1015. https://doi.org/10.1016/j.molcel.2012.12.021.

Xu, Y., and Her, C. (2015). Inhibition of topoisomerase (DNA) I (TOP1): DNA damage repair and anticancer therapy. Biomolecules *5*, 1652–1670. https://doi.org/10.3390/biom5031652.

Yang, G., Mercado-Uribe, I., Multani, A.S., Sen, S., Shih, I.-M., Wong, K.-K., Gershenson, D.M., and Liu, J. (2013). RAS promotes tumorigenesis through genomic instability induced by imbalanced expression of Aurora-A and BRCA2 in midbody during cytokinesis. Int. J. Cancer *133*, 275–285. https://doi.org/10.1002/ijc.28032.

Zeman, M.K., and Cimprich, K.A. (2014). Causes and consequences of replication stress. Nat. Cell Biol. *16*, 2–9. https://doi.org/10.1038/ncb2897.

Zhong, Y., Nellimoottil, T., Peace, J.M., Knott, S.R.V., Villwock, S.K., Yee, J.M., Jancuska, J.M., Rege, S., Tecklenburg, M., Sclafani, R.A., et al. (2013). The level of origin firing inversely affects the rate of replication fork progression. J. Cell Biol. *201*, 373–383. https://doi.org/10.1083/jcb.201208060.

STAR★METHODS

KEY RESOURCES TABLE

REAGENT or RESOURCE	SOURCE	IDENTIFIER
Antibodies		
Mouse anti-BrdU	BD Biosciences	Cat# 347580; AB_10015219
Goat anti-mouse Alexa Fluor 488	Invitrogen	Cat# A11001; AB_2534069
Rat anti-BrdU	Abcam	Cat# ab6326; AB_305426
Goat anti-rat Alexa Fluor 594	Invitrogen	Cat# A11007; AB_10561522
Mouse anti-ssDNA	Millipore	Cat# MAB3034; AB_11212688
Donkey anti-mouse Alexa Fluor 647	Invitrogen	Cat# A31571; AB_162542
Mouse anti-phosphorylated H2AX (Ser 139)	Millipore	Cat# 05-636; AB_309864
Rabbit anti-53BP1	Bethyl Laboratories	Cat# A300-272A; AB_185520
Mouse anti-cyclin A2	Abcam	Cat# ab16726; AB_302478
Mouse anti-S9.6	Kerafast	Cat# ENH001; AB_2687463
Rabbit anti-nucleolin	Abcam	Cat# ab22758; AB_776878
Donkey anti-rabbit Alexa Fluor 488	Abcam	Cat# ab150065; AB_2860569
Goat anti-mouse Alexa Fluor 555	Invitrogen	Cat# A21422; AB_2535844
Rabbit anti-HRAS	Santa Cruz	Cat# sc-520; AB_631670
Mouse anti-Chk1	Cell Signaling	Cat# 2360S
Rabbit anti-phosphorylated chk1 (S345)	Cell Signaling	Cat# 2348S
Rabbit anti-GAPDH	Cell Signaling	Cat# 2118S
Mouse anti-beta Catenin	BD Biosciences	Cat# 610153; AB_397554
Mouse anti-Tubulin	Sigma	Cat# T5168; AB_477579
Mouse anti-beta Actin	Santa Cruz	Cat# sc-69879; AB_1119529
Rabbit anti-Topoisomerase 1	Abcam	Cat# ab109374; AB_10861978
Rabbit anti-RNaseH1	Abcam	Cat# ab229078
Mouse anti-TDP1	Santa Cruz	Cat# sc-365674; AB_10847225
Mouse anti-SRSF1	Santa Cruz	Cat# sc-33652; AB_628248
Donkey anti-rabbit HRP	Jackson ImmunoResearch	Cat# 711-035-152; AB_10015282
Donkey anti-mouse HRP	Jackson ImmunoResearch	Cat# 715-035-150; AB_2340770
Chemicals, peptides, and recombinant proteins		
4-hydroxytamoxifen (4-OHT)	Sigma	Cat# H7904
Guanosine	Sigma	Cat# G6752
Uridine	Sigma	Cat# U3750
Cytidine	Sigma	Cat# C4654
Adenosine	Sigma	Cat# A9251
Aphidicolin (APH)	Sigma	Cat# A0781
Hydroxyurea (HU)	Sigma	Cat# H8627
IdU	Sigma	Cat# I7125
CldU	Sigma	Cat# C6891
RNase III	New England Biolabs	Cat# MO245S
RNaseH1	New England Biolabs	Cat# MO297L
VECTASHILED Antifade mounting medium with DAPI	Vector Laboratories	Cat# H-1200
Colcemid	Biological Industries	Cat# 12-004-1D
EZ-ECL	SARTORUS	Cat# 20500120
Oligofectamine	Invitrogen	Cat# 12252-011
Lipofectamine 2000	Invitrogen	Cat# 11668-027
RNase A	Sigma	Cat# R6513

(*Continued on next page*)

Continued		
REAGENT or RESOURCE	SOURCE	IDENTIFIER
RNaseH2	Dr. Andrew Jackson	N/A
Proteinase K	Sigma	Cat# P2308
SYBER Gold	Invitrogen	Cat# S11494
Camptothecin (CPT)	Sigma	Cat# C9911
Critical commercial assays		
Fiber-Prep kit	Genomic Vision	Cat# EXTR-001
Fiber-Comb kit	Genomic Vision	Cat# MSC-001
Crystal violet assay kit	Abcam	Cat# ab121855
Deposited data		
Raw and analyzed RNA-seq data	This paper	GSE168738
Experimental models: Cell lines		
FSE hTert	Dr. Yehuda Tzfati	N/A
WI-38 hTert	Dr. Amir Eden	N/A
HEK-293	Dr. Michal Goldberg	N/A
Oligonucleotides		
PCR GAPDH Fwd: TGAGCTTGACAAAGTGGTCG	Hy Labs	N/A
PCR GAPDH Rev: GGCTCTCCAGAACATCATCC	Hy Labs	N/A
PCR POLR2A Fwd: TGCGCACCATCAAGAGAGTC	Hy Labs	N/A
PCR POLR2A Rev: CTCCGTCACAGACATTCGCTT	Hy Labs	N/A
PCR TOP1 Fwd: CCCTGTACTTCATCGACAAGC	Hy Labs	N/A
PCR TOP1 Rev: CCACAGTGTCCGCTGTTTC	Hy Labs	N/A
siTOP1-1: GCACAUCAAUCUACACCCA	Dharmacon	Cat# S0-2605017G
siTOP1-2: CGAAGAAGGUAGUAGAGUC	Dharmacon	Cat# S0-2605017G
siSRSF1-1: UUCGGAUGUCUGGAGGUAAGUUACC	Invitrogen	Cat# HSS109654
siSRSF1-2: GGACAUUGAGGACGUGUUCUACAAA	Invitrogen	Cat# HSS109655
siCtrl: UGGUUUACAUGUCGACUAA	Dharmacon	Cat# D-001810-01-20
DRIP RPL13A Fwd: GCTTCCAGCACAGGACAGGTAT	This paper	N/A
DRIP RPL13A Rev: CACCCACTACCCGAGTTCAAG	This paper	N/A
DRIP PRKG1 Fwd: TGTATTCTAACCAGACCTCCTAAATTGG	This paper	N/A
DRIP PRKG1 Rev: AGTGGTCAGTGGCCTTTTGG	This paper	N/A
DRIP SAV1 Fwd: CTGTGTCCTCACCCAAATCTCAT	This paper	N/A
DRIP SAV1 Rev: CCAGGTCCCTCCCTTGATACA	This paper	N/A
Recombinant DNA		
ER:RAS pLNC	Dr. Juan Carlos Acosta	N/A
pEF1-GFP-TOP1	Dr. Tasuku Honjo	N/A
pEGFP-RNaseH1	Dr. Robert Crouch	N/A
pGFP-TDP1	Dr. Fritz Boege	N/A
pEF1-GFP	Dr. Tasuku Honjo	N/A
Software and algorithms		
ImageJ	Schneider et al., 2012	https://imagej.nih.gov/ij/
Prism 8.3.0	GraphPad	https://www.graphpad.com/
RStudio	RStudio Team	https://www.rstudio.com/

RESOURCE AVAILABILITY

Lead contact

Further information and requests for resources and reagents should be directed to and will be fulfilled by the lead contact, Batsheva Kerem (batshevak@savion.huji.ac.il).

Materials availability

This study did not generate new unique reagents.

Data and code availability

- All RNA-seq data were deposited at GEO and are publicly available as of the date of publication. Accession number is listed in the key resources table.
- This paper does not report original code.
- Any additional information required to reanalyze the data reported in this paper is available from the lead contact.

EXPERIMENTAL MODEL AND SUBJECT DETAILS

Cell Culture

Male human foreskin fibroblasts, FSE-hTert cells; female lung fibroblasts, WI38-hTert; and HEK-293 cells originating from a female fetus were grown in DMEM supplemented with 10% fetal bovine serum, 100,000 U l^{-1} penicillin and 100 mg L^{-1} streptomycin. ER:RAS activation was induced by supplementing the growth media with 200 μM of 4-hydroxytamoxifen (4-OHT). Nucleoside supplementation was achieved by supplementing the growth media with 50 μM of A, U, C and G each for 48 h prior to fixation. Aphidicolin and hydroxyurea treatments were performed in growth media with indicated concentrations for 48 h prior to fixation.

Plasmids

For ER:RAS infection, Phoenix retroviral packaging cells were transiently transfected with ER:RAS pLNC vector plasmids (kindly provided by Dr. J.C Acosta). Cells were infected three times with the Phoenix cell supernatant, containing replication-defective viruses. Infected FSE and WI38 cells were selected using 400 μg mL^{-1} G418 for the next 10 days. For TOP1-GFP transfection, HEK-293 cells were transiently transfected with pEGFP-TOP1 or with a control pEF1-GFP vector (kindly provided by Dr. Tasuku Honjo). Transfected cells were FACS sorted 24 h post transfection and 24 h later GFP positive cells were analyzed. For GFP-RNaseH1 transfection, HEK-293 cells were transiently transfected with pEGFP-RNaseH1 vector (kindly provided by Dr. Robert Crouch) or with a control pEF1-GFP vector. Transfected cells were FACS sorted 24 h post transfection and 48 h later GFP positive cells were analyzed. For GFP-TDP1 transfection, HRK-293 cells were transiently transfected with pGFP-TDP1 vector (kindly provided by Dr. Fritz Boege) or with a control pEF1-GFP vector. Transfected cells were FACS sorted 24 h post transfection and 48 h later GFP positive cells were analyzed.

METHOD DETAILS

Replication dynamics using DNA combing

Molecular combing is a process whereby single DNA molecules (hundreds of Kbs) are stretched on a silanized glass surface (COV-002, Genomic vision) (Bensimon et al., 1994). In general, unsynchronized cells were labeled for 30 min by medium containing 100 μM of the thymidine analog iododeoxyuridine (IdU). At the end of the first labeling period, the cells were washed twice with a warm medium and pulse labeled once more for 30 min with a medium containing 100 μM chlorodepxyuridine (CldU) and then washed with cold PBS and harvested. Genomic DNA was extracted using Fiber-Prep kit (EXTR-001, Genomic Vision), combed using the Fiber-Comb (MSC-001, Genomic Vision) and analyzed as previously described (Herrick and Bensimon, 1999). The primary antibody for fluorescence detection of IdU was mouse anti-BrdU (Becton Dickinson), and the secondary antibody was goat anti-mouse Alexa Fluor 488 (Invitrogen). The primary antibody for fluorescence detection of CldU was rat anti-CldU (Novus Biologicals). The secondary antibody was goat anti-rat Alexa Fluor 594 (Invitrogen). The primary antibody for fluorescence detection of ssDNA was mouse anti-ssDNA (Millipore). The secondary antibody was donkey anti-mouse Alexa Fluor 647 (Invitrogen). The length of the replication signals and the fork distances were measured in micrometers and converted to kilo bases according to a constant and sequence-independent stretching factor (1μm = 2kb), as previously reported (Herrick and Bensimon, 1999). Fork symmetry is expressed as the ratio of the shorter to the longer distance covered during the IdU pulse, for each pair of sister replication forks. Images were analyzed double blindly using Fiji (Schindelin et al., 2012).

Immunofluorescence staining

Cells were fixed in 4% formaldehyde/PBS for 10 min, permeabilized with 0.5% Triton/PBS for 10 min, and blocked with 10% fetal bovine serum/PBS for 1-3 h. The primary antibodies used were mouse anti-phosphorylated H2AX (Millipore, 1:100), rabbit anti-53BP1 (Bethyl Laborartories, 1:100), mouse anti-cyclin A2 (Abcam, 1:100) and mouse anti-BrdU (Becton Dickinson, 1:25). For RNA-DNA hybrid detection, cells were washed with cold PBS and incubated with pre-fixation buffer solution (0.5% Triton X-100, 20mM Hepes-KOH pH 7.9, 50mM NaCl, 3mM $MgCl_2$, and 300mM Sucrose). After pre-fixation buffer was removed, cells were fixed with 100% ice-cold methanol for 8 min. Then, all cells were treated with RNaseIII (New England Biolabs, MO245S) according to the manufacture instructions for 30 min in 37°c. Washed once with PBS and treated with RNaseH1 (New England Biolabs, MO297L) according to the manufacture instructions for 30 min in 37°c. PBS washed and incubated in blocking solution 2% BSA/PBS overnight.

S9.6 antibody (kindly provided by Dr. Rachel Eiges) was used, 1:500, rabbit anti nucleolin was use at 1:1000 (Abcam). Secondary antibodies added were anti–mouse Alexa Fluor 488 (Invitrogen), anti-rabbit Alexa Fluor 488 (Abcam), anti-mouse Alexa Fluor 555 (Invitrogen). DNA was counterstained with mounting medium for fluorescence with DAPI (Vector Laboratories). For focus information analysis images were taken with the FV-1200 confocal microscope (Olympus, Japan), with a 60X/1.42 oil immersion objective. Multiple dyes sequential scanning mode was used in order to avoid emission bleed-through. For focus and fluorescent intensity analysis the Hermes WiScan system (Idea Bio-Medical, Israel) was used. All images were analyzed double blindly using Fiji (Schindelin et al., 2012).

Metaphase chromosome preparation and fragile site analysis

Cells were treated with 100 ng mL^{-1} colcemid (Invitrogen) for 15–40 min, collected by trypsinization, treated with hypotonic solution at 37°C for 30 min and fixed with multiple changes of methanol:acetic acid 3:1. Fixed cells were kept at −20°c until analysis. For analysis of total gaps and breaks chromosomes were stained with propidium-iodide and analyzed double blindly using Fiji (Schindelin et al., 2012).

Western blot analysis

8-12% polyacrylamide gels were used for protein separation and detection. The gels were transferred to a nitrocellulose membrane, and antibody hybridization and chemiluminescence (ECL) were performed according to standard procedures. The primary antibodies used in these analyses were rabbit anti-H-RAS (Santa Cruz, 1:1,000), mouse anti-CHK1 (Cell signaling, 1:500), rabbit anti-phosphorylated CHK1 (Cell Signaling, 1:200), rabbit anti-GAPDH (Cell Signaling, 1:1,000), mouse anti-β-catenin (BD-Biosciences, 1:2,500), mouse anti-Tubulin (Sigma, 1:50,000), mouse anti- β-Actin (Santa Cruz, 1:2,000), rabbit anti-TOP1 (Abcam, 1:10,000), rabbit anti-RNaseH1 (Abcam, 1:1,000), mouse anti-TDP1(Santa Cruz, 1:500), and mouse anti SRSF1 (Santa Cruz, 1:50). HRP-conjugated anti-rabbit and anti-mouse secondary antibodies was obtained from Jackson Immunoresearch Laboratories (711-035-152, 1:5,000).

Population doublings

Cells were grown in media as indicated in the 'Cell Culture' section. Initial seeding concentration of cells was 10,000 per well. Cells were trypsinized and counted. Population doublings (PD) was measured according to the following formula:

Xb is the number of cells at the beginning of incubation and Xe is the number of cell at the final count (Greenwood et al., 2004).

RNA sequencing analysis

Sequencing libraries were prepared using the Illumina TruSeq mRNA kit, and sequenced (60 bp, single reads) on a single lane of Illumina HiSeq 2500 V4 instrument, to a depth of ~27 million reads per sample. Reads were aligned to the hg19 genome (UCSC, downloaded from iGenomes) using TopHat (v2.0.10) (Kim et al., 2013). HTSeq-count (version 0.6.1p1) (Anders et al., 2015) was used to count reads on gene exons (UCSC Annotation from March 9, 2012). Differential expression analysis was performed using DESeq2 (1.6.3) (Love et al., 2014) with betaPrior set to False. Gene set enrichment analysis was performed using WebGestalt (Wang et al., 2013).

Gene correlation analysis in GEPIA

The online database Gene Expression Profiling Interactive Analysis (GEPIA) (Tang et al., 2017) was used to explore TOP1, NRAS, KRAS, HRAS and MYC expression levels in cancer. GEPIA is an interactive tool for analyzing RNA-seq expression data from 9,736 tumors and 8,587 normal samples from the TCGA and GTEx projects. GEPIA was used to generate TOP1, NRAS, KRAS, HRAS and MYC expression plots in normal and tumor samples and gene expression correlation analysis in tumor samples.

RNA analysis

Total RNA was extracted using the RNeasy Mini Kit extraction kit (QIAGEN). RNA-less and reverse transcriptase-less reactions were used as controls. cDNA synthesis was performed using the High Capacity cDNA Reverse Transcription kit (Applied Biosystems). Real-time PCR was subsequently performed in ABI 7500 using a Power SYBR green PCR master Mix (Applied Biosystems). The expression level was normalized to the transcript levels of GAPDH. Specific primers for these PCRs were designed using the Primer Express software: GAPDH: Fwd, TGAGCTTGACAAAGTGGTCG; Rev, GGCTCTCCAGAACATCATCC, POLR2A: Fwd, TGCGCACCA TCAAGAGAGTC; Rev, CTCCGTCACAGACATTCGCTT, TOP1: Fwd, CCCTGTACTTCATCGACAAGC; Rev, CCACAGTGTCCGC TGTTTC.

siRNA

siRNA against TOP1 (TOP1-1: 5′-GCACAUCAAUCUACACCCA-3′ and TOP1-2: 5′-CGAAGAAGGUAGUAGAGUC-3′) and a control, non-targeting siRNA (Ctrl: 5′-UGGUUUACAUGUCGACUAA-3′) were purchased from Dharmacon. Cells were transfected with 40nM control siRNA and 20nM siRNA against TOP1, using Oligofectamine (Thermo-Fisher). Cells were analyzed 48 h after transfection. siRNA against SRSF1 (Invitrogen HSS109654 and HSS109655). Cells were transfected with 40mM siRNA, using oligofectamie.

Cell cycle analysis

Cells were harvested and the pellet resuspended in 0.5mL cold PBS and fixed in 4.5mL 100% chilled methanol and kept at −20°C. Prior to FACS analysis, methanol residues were washed and cells were resuspended in PBS containing 0.2μg/μl RNase for 30 min. Cells were stained with 50μg/ml propidium iodide and the DNA content was analyzed by flow cytometry (BD FACSAria III).

DRIP-qPCR

DRIP-qPCR was carried out essentially as previously described (García-Rubio et al., 2018) in FSE hTERT ER:RAS cells after 48 h of 200 nM 4-OHT treatment. Briefly, DNA–RNA hybrids were immunoprecipitated using the S9.6 antibody from gently extracted and enzymatically digested DNA, treated or not with RNase H. Quantitative PCR was performed at the indicated regions of RPL13A, PRKG1 and SAV1 genes with the corresponding primers listed below. Means and SEM from at least four independent experiments were calculated.

RPL13A Fwd	GCTTCCAGCACAGGACAGGTAT
RPL13A Rev	CACCCACTACCCGAGTTCAAG
PRKG1 Fwd	TGTATTCTAACCAGACCTCCTAAATTGG
PRKG1 Rev	AGTGGTCAGTGGCCTTTTGG
SAV1 Fwd	CTGTGTCCTCACCCAAATCTCAT
SAV1 Rev	CCAGGTCCCTCCCTTGATACA

Alkaline gel electrophoresis

To determine the presence of excess genome-embedded ribonucleotides in nuclear DNA, alkaline gel electrophoresis of RNaseH2-treated genomic DNA was performed as previously described (Reijns et al., 2022). MEF RNaseH2B$^{+/+}$ and RNaseH2B$^{-/-}$ were used as controls (Reijns et al., 2012). Total nucleic acids were isolated from pellets from ~1 million cells by incubation in ice-cold buffer (20mM TRIs-HCl ph7.5, 75mM NacCl, 50 mM EDTA) with 200 μg mL^{-1} proteinase K (Sigma) for 10 min on ice, followed by addition of *N*-lauroylsarcosine sodium salt to a final concentration of 1%. Nucleic acids were extracted using phenol-chloroform, then isopropanol-precipitated and dissolved in nuclease-free water. For alkaline gel electrophoresis, 500 ng of total nucleic acids was incubated with 1pmol of purified recombinant RNaseH2 (kindly provided by Dr. Martin Reijns and Prof. Andrew Jackson, (Reijns et al., 2011)) and 0.25 μg of RNaseA (Sigma) for 30 min at 37c in 100 μL reaction buffer (60 mM KCl, 39mM Tris-HCl pH 8.0, 1.5 mM $MgCl_2$, 0.01% Triton X-100). Nucleic acids were ethanol-precipitated, dissolved in nuclease-free water and 250 ng was separated on 0.7% agarose gels in 50 mM NaOH, 1 mM EDTA. After overnight electrophoresis the gel was neutralized in 0.7 M Tris-HCl pH 8.0, 1.5 M NaCl and stained with SYBER Gold (Invitrogen). Images were taken with ChemiDoc Bio-Rad, and densitometry plots were generated using ImageJ (Schindelin et al., 2012).

Mutation analysis

Expression and mutational data were collected from ICGC data portal (ref). Briefly, TOP1 expression in normal (healthy) samples was used to determine TOP1 expression profile; such that expression > 2SD of the mean were considered high-TOP1 and samples within the range ±2SD of the mean were considered normal-TOP1. Then, tumor samples were divided into 2 groups according to their TOP1 expression profile (normal or high). Indel and SBS count per sample were compared between normal- and high-TOP1. Indel and SBS profiles in normal-TOP1, high-TOP1 and high-normal (subtracted) were calculated based on the relative percentage of each mutation type per sample. The relative contribution of indel and SBS signatures to the mutational profiles was performed using YASPA package for R (Hübschmann et al., 2021).

Viability assay

Control and RAS-expressing cells for 3 days were seeded in 96 wells, and treated with camptothecin (CPT, Sigma) 0.0001-1 μM for 3 days. Cristal Violet staining assay was performed according to manufacturer's instructions (Abcam, ab232855). Briefly, Cells were washed with a washing solution and then stained with Crystal Violet for 20 min in RT°c. Staining solution was removed, and cells were washed four times with washing solution, followed by incubation with solubilization solution for 20 min in RT°c. O.D was measured by Synergy H1 plate reader.

QUANTIFICATION AND STATISTICAL ANALYSIS

All data analysis was performed using Excel, GraphPad Prism 8.3.0 for Windows, GraphPad Software, La Jolla California USA (www.graphpad.com) or R project for Statistical Computing (htpp://www.r-project.com). For comparisons of replication dynamics, Immunofluorescence staining, metaphase spreads analyses, and SA-β gal activity student t-test, one-way ANOVA and Mann-Whitney rank-sum test were performed, as indicated. Numbers of repeats are indicated in the figure legends.